

SYMBOL SYNCHRONIZATION FOR MSK SIGNALS  
BASED ON MATCHED FILTERING

A THESIS SUBMITTED TO  
THE GRADUATE SCHOOL OF NATURAL AND APPLIED SCIENCES  
OF  
THE MIDDLE EAST TECHNICAL UNIVERSITY

BY

SERDAR SEZGİNER

IN PARTIAL FULFILMENT OF THE REQUIREMENTS FOR THE DEGREE OF  
MASTER OF SCIENCE

IN

THE DEPARTMENT OF ELECTRICAL AND ELECTRONICS ENGINEERING

SEPTEMBER 2003

Approval of the Graduate School of Natural and Applied Sciences

---

Prof. Dr. Canan Özgen  
Director

I certify that this thesis satisfies all the requirements as a thesis for the degree of Master of Science.

---

Prof. Dr. Mübeccel Demirekler  
Head of Department

This is to certify that we have read this thesis and that in our opinion it is fully adequate, in scope and quality, as a thesis for the degree of Master of Science.

---

Prof. Dr. Yalçın Tanık  
Supervisor

Examining Committee Members

Assoc. Prof. Dr. Melek D. Yücel (Chairman)

Prof. Dr. Yalçın Tanık

Prof. Dr. Kerim Demirbaş

Prof. Dr. Mete Severcan

Dr. Alime (Yanartaş) Özyıldırım

## **ABSTRACT**

### **SYMBOL SYNCHRONIZATION FOR MSK SIGNALS BASED ON MATCHED FILTERING**

**Sezginer, Serdar**

**M.Sc., Department of Electrical and Electronics Engineering**

**Supervisor: Prof. Dr. Yalçın Tanık**

**September 2003, 83 pages**

In this thesis, symbol timing recovery in MSK signals is investigated making use of matched filtering. A decision-directed symbol synchronizer cascaded with an MLSE receiver is proposed for fine timing. Correlation (matched filter) method is used to recover the timing epoch from the tentative decisions obtained from the Viterbi algorithm. The fractional delays are acquired using interpolation and an iterative maximum search process. In order to investigate the tracking performance of the proposed symbol synchronizer, a study is carried out on three possible optimum timing phase criteria: (i) Mazo criterion, (ii) the minimum squared ISI criterion (msISI), and (iii) the minimum BER criterion. Moreover, a discussion is given about the timing sensitivity of the MLSE receiver. The performance of the symbol synchronizer is assessed by computer simulations. It is observed that the proposed synchronizer tracks the variations of the channels almost the same as the msISI criterion. The proposed method eliminates the cycle slips very successfully and is robust to frequency-selective multipath fading channel conditions even in moderate signal-to-noise ratios.

**Keywords:** symbol timing, minimum shift keying (MSK), matched filtering, optimum timing phase, Viterbi algorithm, multipath fading

## ÖZ

### MSK SİNYALLERİ İÇİN UYUMLU SÜZGEÇLEMeye DAYALI SEMBOL EŞZAMANLAMASI

Sezginer, Serdar

Yüksek Lisans, Elektrik ve Elektronik Mühendisliği Bölümü

Tez Yöneticisi: Prof. Dr. Yalçın Tanık

Eylül 2003, 83 sayfa

Bu tezde, en küçük kaydırmalı kiplenim (MSK) sinyalleri için uyumlu süzgeçleme kullanılarak sembol zaman bilgisinin kazanımı incelenmiştir. Hassas zamanlama için karara bağlı en büyük olasılıklı dizi kestirimi (MLSE) almacı ile birleştirilmiş bir sembol eşzamanlayıcısı önerilmiştir. Zaman birimi Viterbi algoritmasından elde edilen kesin olmayan kararlarla ilinti (uyumlu süzgeç) yöntemi kullanılarak kazanılmıştır. Ufak zaman gecikmeleri aradeğerleme ve döngülü en yüksek arama ile elde edilmiştir. Önerilen sembol eşzamanlayıcısının başarımını incelemek amacı ile olası en iyi üç zamanlama evresi ölçütü üzerine bir çalışma yapılmıştır: (i) Mazo ölçütü, (ii) en küçük karesi alınmış ISI (msISI) ölçütü, ve (iii) en küçük BER ölçütü. Ayrıca, MLSE almacının zamanlama duyarlılığından bahsedilmiştir. Sembol eşzamanlayıcısının başarımı bilgisayar benzetimleri kullanılarak değerlendirilmiştir. Önerilen eşzamanlayıcının kanal değişimlerini msISI ölçütüne çok benzer takip ettiği gözlenmiştir. Önerilen yöntem devir kaymalarını başarıyla elemektedir ve ortalama sinyal-gürültü oranında bile frekansa bağımlı çokyollu sönümlemeli kanallarda gürbüzdür.

**Anahtar kelimeler:** sembol zaman bilgisi, en küçük kaydırmalı kiplenim, uyumlu süzgeçleme, en iyi zamanlama evresi, Viterbi algoritması, çokyollu sönümleme

*To my family...*

## **ACKNOWLEDGMENTS**

I am greatly indebted to my supervisor Prof. Dr. Yalçın Tanık for his valuable guidance and encouragement. He shared with me not just his technical experience but also his philosophical insights which I have benefited greatly.

I would also like to express my deep gratitude to my parents and my dear brother, for their support, understanding and patience throughout my education life.

Special thanks are due to Bilgi Aktürk for her support and encouragement. Further, I would like to acknowledge the motivative discussions and friendship of my colleagues Ülkü Çilek and Özgür Ertuğ during my graduate study.

## TABLE OF CONTENTS

<b>ABSTRACT</b> .....	<b>iii</b>
<b>ÖZ</b> .....	<b>iv</b>
<b>ACKNOWLEDGMENTS</b> .....	<b>vi</b>
<b>TABLE OF CONTENTS</b> .....	<b>vii</b>
<b>LIST OF TABLES</b> .....	<b>ix</b>
<b>LIST OF FIGURES</b> .....	<b>x</b>
<b>LIST OF ABBREVIATIONS</b> .....	<b>xiii</b>
<b>CHAPTER</b> .....	<b>1</b>
<b>1. INTRODUCTION</b> .....	<b>1</b>
1.1. Scope and Objective.....	1
1.2. Outline of the Thesis .....	3
<b>2. CHANNEL MODEL AND MLSE RECEIVER</b> .....	<b>5</b>
2.1. Introduction .....	5
2.2. Channel Model .....	5
2.2.1. Characterization of Multipath Fading Channel .....	6
2.2.2. Channel Modelling .....	7
2.2.2.1. Doppler Spectrum Type .....	8
2.2.2.2. Power Delay Profile .....	9
2.3. MLSE Receiver for MSK Signals in Multipath Fading Channels .....	12
2.3.1. MSK Signals and Derotation.....	12
2.3.2. MLSE Receiver and Viterbi Algorithm .....	15
<b>3. SYMBOL SYNCHRONIZATION REVIEW</b> .....	<b>20</b>
3.1. Introduction .....	20
3.1.1. Symbol Timing Recovery .....	20
3.1.2. Existing STR Schemes .....	22

3.2.	Symbol Synchronization in MSK Signals.....	25
3.3.	Maximum Likelihood Timing Estimation.....	28
3.4.	Modified Cramér-Rao Bound.....	32
<b>4.</b>	<b>A DD STR BASED ON MATCHED FILTERING FOR MSK SIGNALS.....</b>	<b>34</b>
4.1.	Introduction .....	34
4.2.	Optimum Value Criteria for Timing Phase .....	35
4.2.1.	Mazo Criterion .....	35
4.2.2.	Minimum Squared ISI (msISI) Criterion .....	38
4.2.3.	Minimum BER Criterion.....	41
4.3.	Proposed DD STR for MSK Signals.....	44
4.3.1.	Correlation (Matched Filter) Method .....	44
4.3.2.	Interpolation .....	46
4.3.3.	Iterative Maximum Search .....	49
4.3.4.	Discussion on Performance of the Proposed STR Scheme .....	50
<b>5.</b>	<b>SIMULATION &amp; RESULTS .....</b>	<b>56</b>
5.1.	Introduction .....	56
5.2.	Simulation Model of the Communication System .....	56
5.2.1.	Simulated Channel Specifications.....	57
5.2.2.	Receiver Structure .....	58
5.3.	Tracking Performance of the Symbol Synchronizer .....	59
<b>6.</b>	<b>CONCLUSION.....</b>	<b>69</b>
	<b>REFERENCES .....</b>	<b>71</b>
	<b>APPENDICES .....</b>	<b>75</b>
<b>A.</b>	<b>CPM SIGNALS .....</b>	<b>75</b>
A.1.	Signal Model .....	75
A.2.	Linearization of CPM Signals .....	76
<b>B.</b>	<b>ERROR PERFORMANCE OF THE MLSE RECEIVER.....</b>	<b>79</b>

## LIST OF TABLES

### TABLE

4.1	Normalized timing standard deviation for $L_0 = 15$ .....	53
4.2	Normalized timing standard deviation for $L_0 = 30$ .....	53

## LIST OF FIGURES

FIGURE	
2.1	Multipath fading channel model..... 7
2.2	Classical Doppler Spectrum ( $f_d = 150$ Hz). ..... 9
2.3	A TU Channel Power Delay Profile..... 10
2.4	Adjustment of the spectrum of a tap weight..... 10
2.5	Rayleigh fading envelope ( $f_d = 150$ Hz). ..... 12
2.6	Pulse shape of linearized MSK signal..... 13
3.1	Typical block diagram of a baseband receiver..... 21
3.2	Feedback configuration. .... 23
3.3	Feedforward configuration..... 23
3.4	Synchronous sampling. .... 24
3.5	Effect of timing errors on MSK modulation. .... 28
4.1	Normalized timing phase obtained from Mazo criterion ( $v = 50$ km/h, $f_c = 900$ MHz)..... 37
4.2	Normalized timing phase obtained from Mazo criterion ( $v = 90$ km/h, $f_c = 1800$ MHz)..... 38
4.3	Comparison between the timing values obtained from msISI and Mazo criteria ( $v = 50$ km/h, $f_c = 900$ MHz). .... 40

4.4	Comparison between the timing values obtained from msISI and Mazo criteria ( $v = 90$ km/h, $f_c = 1800$ MHz). .....	40
4.5	Timing values obtained from the maximization of the minimum distance. ....	42
4.6	Minimum distance comparison between minimum BER and msISI criteria. ....	43
4.7	Impulse response of raised cosine filter. ....	47
4.8	Illustration of $k$ and $\tau$ in determining the timing instant. ....	48
4.9	Illustration of the iteration process by Bisection Method. ....	50
4.10	Normalized timing standard deviation for different SNR values. ....	51
4.11	Matched filter output, SNR = 30 dB. ....	52
4.12	Matched filter output, SNR = 30 dB, fading channel. ....	54
4.13	General flow in the proposed timing recovery scheme. ....	55
5.1	General block diagram of the simulated system. ....	57
5.2	Performance of the symbol synchronizer in AWGN channel. ....	60
5.3	Performance of the symbol synchronizer for different interpolation lengths in AWGN channel ( $L_0 = 15$ ). ....	61
5.4	Performance of the symbol synchronizer for different interpolation lengths in AWGN channel ( $L_0 = 30$ ). ....	61
5.5	Tracking performance of the proposed scheme ( $L_0 = 30$ , SNR = 30 dB, $v = 50$ km/h, $f_c = 900$ MHz). ....	62
5.6	Tracking performance of the proposed scheme ( $L_0 = 30$ , SNR = 20 dB, $v = 50$ km/h, $f_c = 900$ MHz). ....	63

5.7	Tracking performance of the proposed scheme ( $L_0 = 20$ , SNR = 30 dB, $v = 50$ km/h, $f_c = 900$ MHz). .....	64
5.8	Tracking performance of the proposed scheme ( $L_0 = 30$ , SNR = 30 dB, $v = 90$ km/h, $f_c = 1800$ MHz). .....	65
5.9	Tracking performance of the proposed scheme ( $L_0 = 20$ , SNR = 30 dB, $v = 90$ km/h, $f_c = 1800$ MHz). .....	65
5.10	Tracking performance of the proposed scheme ( $L_0 = 30$ , SNR = 30 dB, $v = 90$ km/h, $f_c = 1800$ MHz). .....	66
5.11	Comparison between msISI and Mazo criteria ( $L_0 = 30$ , SNR = 30 dB, $v = 90$ km/h, $f_c = 1800$ MHz). .....	67
5.12	Tracking performance in the presence of a cycle slip ( $L_0 = 30$ , SNR = 30 dB, $v = 90$ km/h, $f_c = 1800$ MHz). .....	68

## LIST OF ABBREVIATIONS

AWGN	Additive White Gaussian Noise
BER	Bit Error Rate
CIR	Channel Impulse Response
CPM	Continuous Phase Modulation
CRB	Cramér-Rao Bound
DA	Data-Aided
DD	Decision-Directed
FB	Feedback
FF	Feedforward
GMSK	Gaussian Minimum Shift Keying
ISI	Intersymbol Interference
LLF	Log Likelihood Function
MAP	Maximum A Posteriori
MF	Matched Filter
ML	Maximum Likelihood
MLSE	Maximum Likelihood Sequence Estimation
MMSE	Minimum Mean Square Error
MSK	Minimum Shift Keying
NDA	Non-Data-Aided
PDF	Probability Density Function
PLL	Phase Locked Loop
SNR	Signal-to-Noise Ratio
STR	Symbol Timing Recovery
VA	Viterbi Algorithm

# CHAPTER 1

## INTRODUCTION

### 1.1. Scope and Objective

In digital radio communications, the demand for reliable, high-speed and high-quality transmission has led to an investigation of various receiver design techniques. In order to determine the most suitable digital communication system, every stage of the system has taken considerable attention. Symbol synchronization or symbol timing recovery (STR) is one of the most critical receiver functions in synchronous communication systems. Proper recovery and tracking of the symbol timing are of crucial importance and necessary in the demodulation and data detection for good performance.

The ideal timing phase for a given system depends on the overall impulse response and thus on the characteristics of the communication channel. Multipath fading with large delay spread, typically in urban area, introduces intersymbol interference (ISI) in addition to the ambiguous delay in the transmission. Because of this reason, determination of the proper sampling instants is one of the most difficult problems in time-dispersive channels and an accurate analysis is extremely difficult, if not possible. Most of the practical synchronizers are based on heuristic algorithms that have been based on transmission systems with no intersymbol interference (ISI) or with a time spread less than a symbol period which is not so realistic for bandlimited channels.

For the recovery of the timing information in the presence of severe channel effects, specifically designed synchronizers are needed. Feedforward approaches based on maximum likelihood (ML) estimation are good candidates,

because of their rapid acquisition of symbol timing with the absence of hang-up problems, which is common in feedback structures. Through the extensive research on these approaches, the trend of designing receivers for bandwidth efficient continuous phase modulation (CPM) schemes has created an attractive area for the researchers interested in timing recovery. CPM is a constant envelope, nonlinear modulation method which conserves and reduces energy and bandwidth at the same time [1]. A special form of CPM is MSK which is very attractive for transmission in a mobile radio environment with its constant envelope and relatively narrow bandwidth [2]. In the last two decades, there have been significant attempts on receiver designs for MSK signals including the synchronization aspects. Timing recovery for MSK signals is first discussed by de Buda [3] with a feedback approach. Feedforward approaches for symbol timing estimation for MSK signals are discussed in several papers, [1][4]-[8], but not much attention has been given to the effects of multipath fading on symbol synchronization.

The objective of this thesis is to investigate a timing recovery algorithm for MSK signals, which is able to extract the fractional delays even in the presence of severe channel variations. The recovery of the timing epoch is performed with correlation (matched filter) method together with an interpolator and an iterative maximum search process. In acquisition mode, a data-aided approach is used for the adjustment of the initial timing. Then, tracking is performed with a decision-directed timing recovery. Maximum likelihood sequence estimation (MLSE) with Viterbi algorithm (VA) is used for detection, which is the optimum demodulation technique for data-modulated signals received over a frequency-selective multipath fading channel.

The proposed STR scheme enables the fast and sensitive recovery of the timing epoch. With such a precise timing recovery scheme, the question arises about the optimality in timing recovery. The subject has received attention mainly in early seventies and some possible optimum timing phase criteria are presented in [9]-[11]. Three criteria are discussed in the context of this study; namely, the

Mazo criterion [10], the minimum squared ISI criterion and the minimum BER criterion. Comparing these criteria, the behaviour and the performance of the proposed scheme is observed for different fading channel characteristics.

In summary, the timing recovery is still a problem in time-dispersive channels. The channel effects together with optimality in timing recovery have taken scarce attention. The aim of this thesis study is to design a fast and robust STR scheme for MSK signals with the ability of giving precise timing values even in the presence of severe channel effects and compare its results with possible optimum timing phase criteria.

## **1.2. Outline of the Thesis**

The thesis has the following outline:

In the next chapter, the basic concepts related to the model of the multipath fading channel and the MLSE receiver implemented with VA are presented.

In Chapter 3, the statement of symbol synchronization problem and a review of major symbol timing recovery methods are given. Following this, the maximum likelihood estimation of the timing epoch is reviewed.

The proposed timing recovery scheme is presented in Chapter 4. First, some possible criteria are given for comparison. Then, the correlation (matched filter) method, interpolation and the iterative maximum search algorithm are discussed.

Chapter 5 is devoted to the simulation results. Firstly, the model of the simulated system is given and the details of the simulated chain are presented. Following this, the tracking performance of the proposed scheme is discussed with the simulation results.

In the last chapter, conclusions are drawn and possible future extensions to this work are mentioned.

Signal model and the linearization of CPM are given in Appendix A. Error performance analysis of the MLSE receiver is presented in Appendix B.

## **CHAPTER 2**

### **CHANNEL MODEL AND MLSE RECEIVER**

#### **2.1. Introduction**

In radio channels the delayed and attenuated versions of the transmitted signal are added together at the receiver to produce multipath interference. Each signal path is affected by a random amplitude fade and a phase shift that tends to change over time. Due to the multipath nature of the communication channel, interference occurs between adjacent symbols, which is known as intersymbol interference (ISI). The best theoretical performance for demodulating operations over channels with ISI and additive white Gaussian noise (AWGN) is the maximum likelihood sequence estimation (MLSE) technique which is implemented efficiently by means of Viterbi algorithm (VA).

This chapter addresses a few concepts about the model of the multipath fading channels and the MLSE receiver used in the simulations. First, the channel model is presented with its characterization and simulation modelling. Next, MLSE and the VA are explained, respectively.

#### **2.2. Channel Model**

The mobile radio channel is based on the propagation of radio waves in a complex transmission environment. With a receiver moving around channel appears to be time varying. Since the channel variations as observed by the receiver are random, the channel model is treated as a statistical one.

### 2.2.1. Characterization of Multipath Fading Channel

The physical fading channel can be characterized by the complex-valued time-variant fading channel impulse response (CIR). Most radio channels are illustrated by multipath propagation where a number of reflected or scattered radio rays arrive at the receiving end [12].

Suppose that the transmitted signal is

$$s(t) = \text{Re} \{ s_l(t) e^{j\omega_c t} \}, \quad (2.1)$$

in which  $s_l(t)$  is the complex envelope of the signal. It is assumed that there are multiple propagation paths. A propagation delay and an attenuation factor are associated with each path. Usually the propagation delay changes only slowly with time and may be assumed to remain stationary. Thus, the multipath channel output can be written as

$$x(t) = \sum_n c_n(t) s(t - \Delta t_n), \quad (2.2)$$

where  $\Delta t_n$  is the propagation delay and  $c_n(t)$  is the attenuation factor for the  $n$ -th path. Substitution for  $s(t)$  from equation (2.1) into equation (2.2) yields the result

$$x(t) = \text{Re} \left\{ \left[ \sum_n c_n(t) e^{-j\omega_c \Delta t_n} s_l(t - \Delta t_n) \right] e^{j\omega_c t} \right\}. \quad (2.3)$$

The equivalent low-pass received signal,  $r(t)$  (without noise), is then

$$r(t) = \sum_n c_n(t) e^{-j\omega_c \Delta t_n} s_l(t - \Delta t_n). \quad (2.4)$$

Since  $r(t)$  is the response of an equivalent low-pass channel to the equivalent low-pass signal,  $s_l(t)$ , the equivalent low-pass channel may be expressed by the time-variant impulse response

$$h_c(\Delta t; t) = \sum_n \alpha_n(t) \delta(\Delta t - \Delta t_n), \quad (2.5)$$

where  $h_c(\Delta t; t)$  represents the response of the channel at time  $t$  due to an impulse applied at time  $t - \Delta t$  [13]. Here, the complex random process  $\alpha_n(t)$  is introduced with its amplitude  $c_n(t)$  and phase  $e^{-j\omega_c \Delta t_n}$ . The low-pass equivalent of the fading channel model may be depicted as in Figure 2.1.

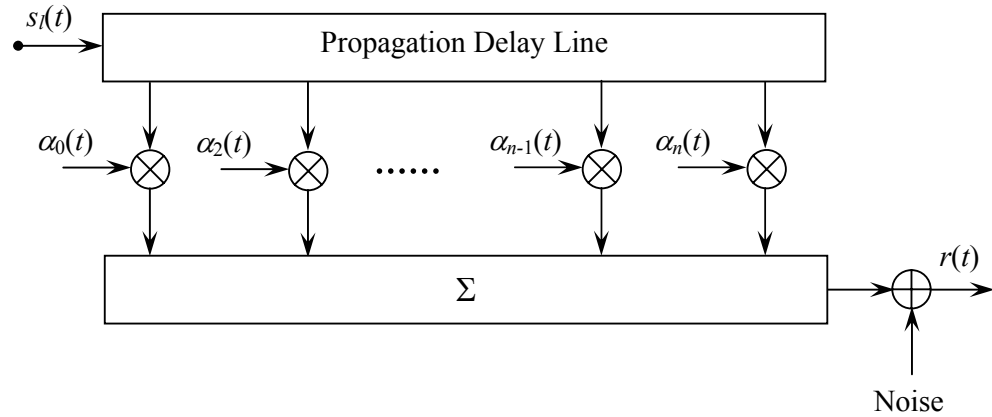


Figure 2.1 Multipath fading channel model.

### 2.2.2. Channel Modelling

For practical simulations, different propagation models can be described by defining discrete number of taps, each determined by their time delay and average power. The time variation of each tap is determined according to a Doppler spectrum, and the average power is adjusted using the power delay profile of the channel. Doppler spectrum and the power delay profile are obtained according to the *scattering function* of the channel [14].

The scattering function is a two dimensional representation of the received signal power as a function of the propagation delay and the Doppler frequency, i.e.,  $S(\Delta t, f)$ . In other words, it describes the manner in which the transmitted power is distributed in time and frequency, upon passing through the channel.

### 2.2.2.1. Doppler Spectrum Type

Simulation of the fading spectrum appropriate to mobile radio communication is obtained by properly shaping the spectrum of the independent noise sources with the Doppler spectrum,  $S(f)$ . It simply determines the time variations of the channel. When  $S(f)$  becomes equal to the delta function  $\delta(f)$ , the channel appears to be time-invariant.

In this thesis, for modelling the time variations of the channel, the well-known classical Doppler spectrum is used. In this spectrum type, all the angle between the vehicle speed and radio waves are assumed to be equally probable. This is the most commonly used, and in a certain sense the worst case Doppler spectrum. It is formulated by the scattering function as

$$\begin{aligned} S_n(f) &= S(\Delta t_n, f) \\ &= \frac{A_n}{\sqrt{1 - \left(\frac{f}{f_d}\right)^2}} \text{ for } f \in (-f_d, f_d), \end{aligned} \quad (2.6)$$

where  $\Delta t_n$  is the propagation delay for the  $n$ -th path.  $f_d = \frac{v}{c} f_c$  represents the maximum Doppler shift, with the vehicle speed  $v$  (m/s), the wavelength  $\lambda(m)$ , and the carrier frequency  $f_c$  [15]. Since the spectra of all the tap weights are assumed to be the same in the simulations, the subscript  $n$  is dropped in the following illustrations. As an example, Classical Doppler spectrum for mobile speed of 90 km/h and with a carrier frequency 1800 MHz is shown in Figure 2.2.

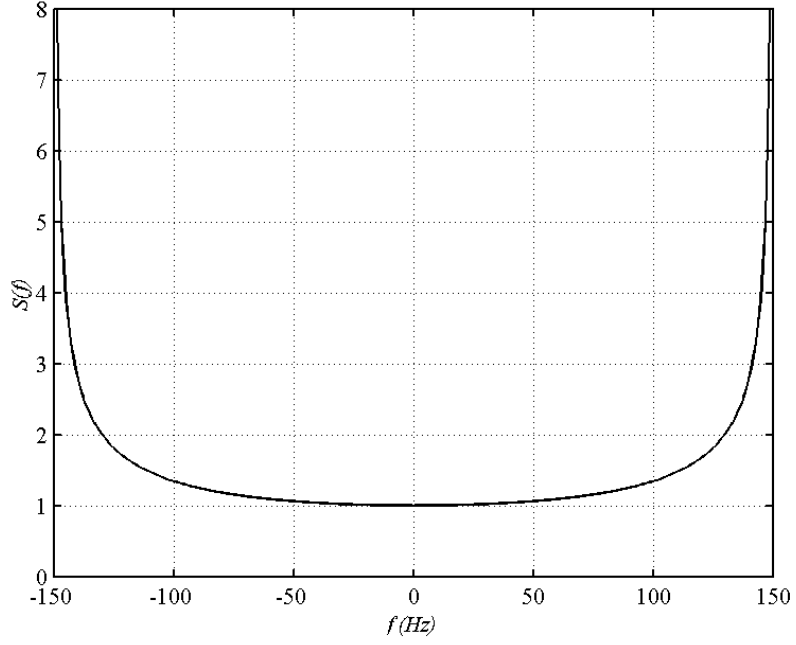


Figure 2.2 Classical Doppler Spectrum ( $f_d = 150$  Hz).

#### 2.2.2.2. Power Delay Profile

The average power for each tap is described by the power delay profile,  $P(\Delta t)$ .

The power delay profiles are defined as [15]

$$P(\Delta t_n) = P_0 \int_{-f_d}^{f_d} S(\Delta t_n, f) df, \quad (2.7)$$

where  $P_0$  is the normalizing power and  $P(\Delta t_n)$  is the power transmitted by tap  $n$ .

As an example, the continuous power delay profile of the simulated channel model is shown in Figure 2.3 with the relation

$$P(\Delta t) = \begin{cases} e^{(-\Delta t)}, & \text{for } 0 < \Delta t < 7 \mu\text{s}, \\ 0, & \text{elsewhere,} \end{cases} \quad (2.8)$$

which is a typical case for urban (non-hilly) area (TU).

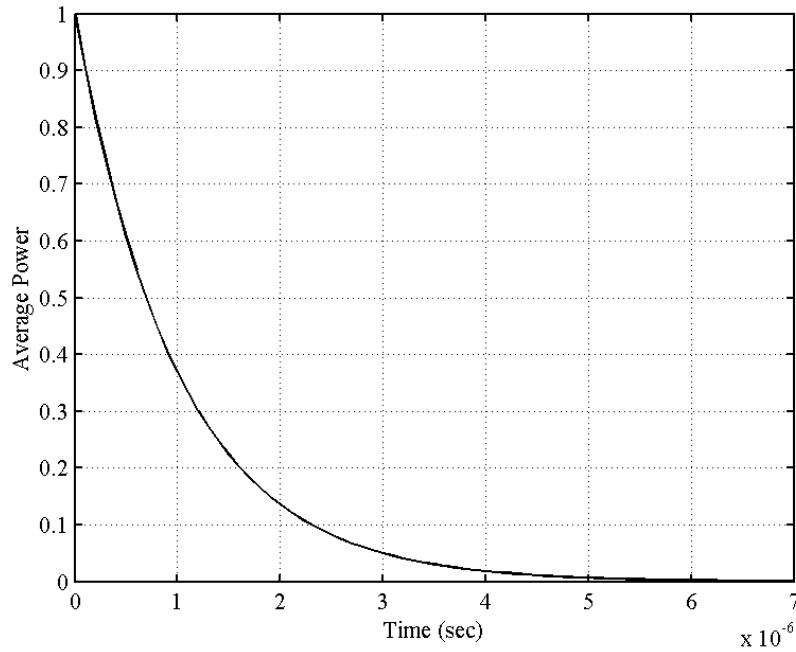


Figure 2.3 A TU Channel Power Delay Profile.

In summary, the variations of the taps are determined by the Doppler spectrum according to (2.6). This is accomplished with adjusting the spectra of the tap weights by filtering the complex white noise,  $w(t)$ , as in Figure 2.4.

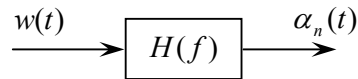


Figure 2.4 Adjustment of the spectrum of a tap weight.

Thus, the power spectral density of the  $n$ -th tap weight can be expressed with the relation

$$S(f) = |H(f)|^2 S_w(f), \quad (2.9)$$

where  $S_w(f)$  is the power spectral density of the white noise. Since the power spectral density of the white noise is a constant (say unity) for all frequencies, the magnitude of the shaping filter response  $H(f)$  becomes

$$|H(f)| = \sqrt{S(f)}. \quad (2.10)$$

As a result, the tap weights may be obtained by filtering the white noise with the shaping filter given in (2.10), together with the power level adjusted according to the power delay profile,  $P(\Delta t)$ , with the relation shown in equation (2.8). Further,  $\alpha_n(t)$ 's are circularly symmetric zero-mean Gaussian processes.

Finally, it is noteworthy to mention that in order to provide Rayleigh distribution for the envelope, two independent Gaussian low-pass noise sources with identical spectra are added in quadrature. The output corresponding to the tap weights then has a Rayleigh distributed envelope and a uniformly distributed phase component. In Figure 2.5, an example of a Rayleigh fading envelope is provided for a Doppler shift of 150 Hz. Notice how the magnitude drops down to a very low level at certain time instants and deep fades occur.

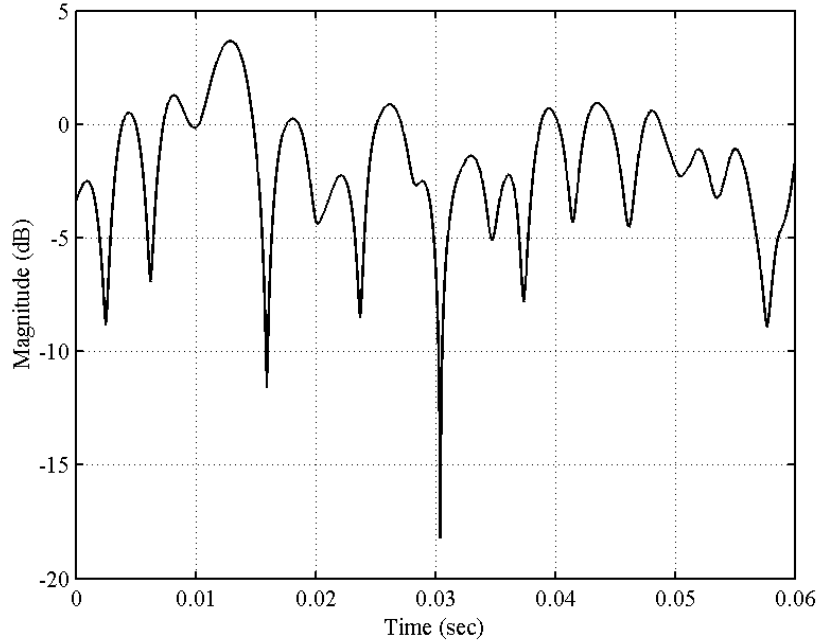


Figure 2.5 Rayleigh fading envelope ( $f_d = 150$  Hz).

### 2.3. MLSE Receiver for MSK Signals in Multipath Fading Channels

In this section, the background information relating the derotation technique employed for the reception of MSK signals, and the MLSE receiver structure implemented with Viterbi algorithm are presented.

#### 2.3.1. MSK Signals and Derotation

MSK modulation type belongs to the class of continuous phase modulations (i.e., binary CPM with modulation index  $h = 1/2$ ) (See Appendix A). This modulation type is essentially nonlinear and classical MLSE algorithms for receiver side cannot be employed directly. However, it has been shown in [16] that binary CPM signals can be represented approximately as pulse amplitude modulated (PAM) signals by adopting a suitable pulse shape. Hence, as shown in Appendix A, baseband equivalent MSK signals can be expressed exactly as

$$s_l(t) = \sum_{i=-\infty}^{\infty} \exp\left(j \frac{\pi}{2} \sum_{k=-\infty}^i b_k\right) g(t - iT), \quad (2.11)$$

where  $g(t)$  denotes the real-valued pulse shaping function and  $b_k$ 's  $\in \{\pm 1\}$  are the input data bits to the modulator. The energy constant  $\sqrt{2E_s/N_0}$  is dropped for convenience. For MSK signal,  $g(t)$  is a one half cycle sinusoid with duration of two symbol periods as shown in Figure 2.6.

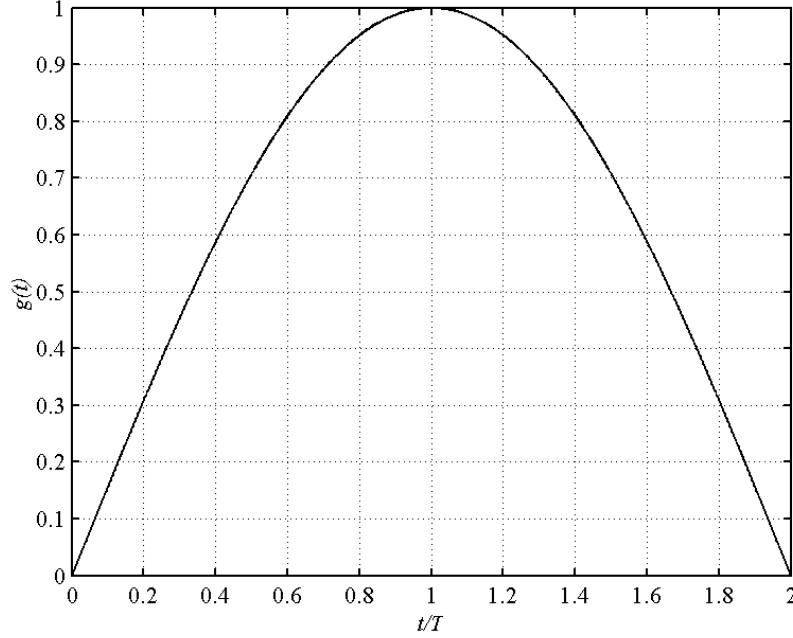


Figure 2.6 Pulse shape of linearized MSK signal.

As in GSM system, for ease in implementation, the data to the modulator is precoded by the rule  $b_k = a_k a_{k-1}$ , where  $a_k$ 's  $\in \{\pm 1\}$  are the original information bits. Using this property and assuming that the data sequence be defined for  $k \geq i_0$  in (2.11) [17] gives

$$\begin{aligned}
 s_i(t) &= \sum_{k=i_0}^{\infty} \exp\left(j \frac{\pi}{2} \sum_{k=i_0}^i a_k a_{k-1}\right) g(t - iT) \\
 &= \sum_{i=i_0}^{\infty} \prod_{k=i_0}^i \exp\left(j \frac{\pi}{2} a_k a_{k-1}\right) g(t - iT). \tag{2.12}
 \end{aligned}$$

Using the equality  $\exp(j\frac{\pi}{2}a_k a_{k-1}) = ja_k a_{k-1}$ , equation (2.12) can be rewritten as

$$s_l(t) = \sum_{i=i_0}^{\infty} \prod_{k=i_0}^i ja_k a_{k-1} g(t-iT) = \sum_{i=i_0}^{\infty} j^{(i-i_0+1)} \prod_{k=i_0}^i a_k a_{k-1} g(t-iT). \quad (2.13)$$

Since  $\prod_{k=i_0}^i a_k a_{k-1} = a_i a_{i_0-1} \prod_{k=i_0}^{i-1} a_k^2$  and  $a_k^2 = 1$  for all  $k$ , we get

$$s_l(t) = j^{(i-i_0+1)} a_{i_0-1} \sum_{i=i_0}^{\infty} a_i j^i g(t-iT). \quad (2.14)$$

Finally, assuming the terms  $a_{i_0-1} = 1$  and  $j^{(i-i_0+1)} = 1$  which are independent of  $i$  and letting  $i_0 \rightarrow -\infty$ , the general result is obtained as

$$s_l(t) = \sum_{i=-\infty}^{\infty} a_i j^i g(t-iT). \quad (2.15)$$

The signal at the receiver will in general have passed through a frequency-selective channel with a complex impulse response  $h_c(t)$ , and a receiver filter with an impulse response  $g_R(t)$  in order to reduce adjacent channel interference and noise. The received signal then becomes (in the absence of noise)

$$r(t) = \sum_{i=-\infty}^{\infty} a_i j^i h(t-iT), \quad (2.16)$$

where  $h(t) = g(t) \otimes h_c(t) \otimes g_R(t)$  is the overall impulse response of the system from the source to the detector input where  $\otimes$  denotes convolution. The received signal possesses a rotational structure because of the factor  $j^i$  in the equation (2.16). This causes a  $\pi/2$  phase rotation on the complex plane from symbol to symbol. This can be avoided by means of a derotation technique, [18], by

multiplying the received signal by the complex function:  $q(t) = (-j)^i$  for  $iT \leq t < (i+1)T$ . Finally, the signal takes the form

$$r_d(t) = q(t)r(t) = \sum_i a_i h_d(t - iT) \quad (2.17)$$

with the derotated impulse response  $h_d(t) = q(t)h(t)$ . Thus, the rotational structure of the signal  $r(t)$  is removed and a linear PAM receiver model can be obtained. The form of  $r_d(t)$  given in (2.17) allows classical MLSE detection of the transmitted data sequence by the use of Viterbi algorithm (See Section 2.3.2). In the sequel, the subscripts indicating the derotation will be dropped for convenience.

### 2.3.2. MLSE Receiver and Viterbi Algorithm

The conventional MLSE receiver generally consists of an ML sequence estimator implemented by the Viterbi algorithm (VA). Viterbi algorithm uses the knowledge of channel characteristics and of the received signal in order to find the most likely transmitted data sequence. The algorithm does not attempt to equalize the received waveform, so that the performance of this receiver is dependent on the available estimate of the channel impulse response (CIR). Throughout the study, the perfect estimation of the channel is assumed.

In the previous section, it is shown that the received signal can be expressed as the convolution of the transmitted data bits with the overall impulse response. Thus, including the additive noise of the transmission medium, the received signal can be expressed as

$$r(t) = \sum_{k=0}^{K-1} a_k h(t - kT) + w(t), \quad (2.18)$$

where  $a_k$ 's  $\in \{\pm 1\}$  are the transmitted bits,  $w(t)$  is the white Gaussian noise process, and  $K$  is the observation interval in symbols.  $h(t)$  is the overall system

impulse response after derotation which accounts for the pulse shaping of the modulation, selectivity of the channel and the receiver filter.

With the assumption that the function  $h(t)$  is known, the received signal in the absence of noise may be reconstructed for each possible sequence. Let the reconstructed complex baseband signal for the  $m$ -th sequence be denoted as

$$s_m(t) = \sum_{k=0}^{K-1} a_k^m h(t - kT). \quad (2.19)$$

The MLSE algorithm attempts to find the transmitted sequence  $\vec{a} = [a_0 \ a_1 \ \dots \ a_{K-1}]$  that maximizes the log likelihood function (LLF) [13]

$$\ln[p_{r(t)\vec{a}}(r(t) | \vec{a})]_{\infty} - \int_{-\infty}^{\infty} \left| r(t) - \sum_{k=0}^{K-1} a_k h(t - kT) \right|^2 dt. \quad (2.20)$$

The direct solution of this maximization problem is to select the one among the  $M = 2^K$  possible vectors  $\vec{a}$  which maximizes (2.20). It is obvious that as the length of the transmitted vector  $\vec{a}$  gets larger, the maximization of the LLF function becomes computationally inefficient. To reduce this computational load Viterbi algorithm can be used.

In the literature, there are basically two approaches for the application of the Viterbi algorithm to this problem. One of them is by Forney [19] and the other by Ungerboeck [20]. The Forney's approach follows the standard Viterbi algorithm and theoretically requires the whitening filter. On the other hand, Ungerboeck's approach directly uses the non-whitened samples. In this study, the receiver structure proposed by Ungerboeck is considered which includes a matched filter and a modified VA.

If we turn our attention to the LLF again, we see that maximizing (2.20) for the  $m$ -th sequence is equivalent to maximizing the function

$$\Lambda_m = 2 \operatorname{Re} \sum_{k=0}^{K-1} \left[ (a_k^m)^* \int_{-\infty}^{\infty} r(t) h^*(t - kT) dt \right] - \sum_{k=0}^{K-1} \sum_{i=0}^{K-1} (a_k^m)^* a_i^m \int_{-\infty}^{\infty} h^*(t - kT) h(t - iT) dt. \quad (2.21)$$

We may rewrite equation (2.21) as

$$\Lambda_m = 2 \operatorname{Re} \left[ \sum_{k=0}^{K-1} (a_k^m)^* y_k \right] - \sum_{k=0}^{K-1} \sum_{i=0}^{K-1} (a_k^m)^* x_{k-i} a_i^m, \quad (2.22)$$

where

$$y_k = y(kT) = \int_{-\infty}^{\infty} r(t) h^*(t - kT) dt, \quad (2.23)$$

$$x_k = x(kT) = \int_{-\infty}^{\infty} h^*(t) h(t + kT) dt. \quad (2.24)$$

In words,  $y_k$  is a sample taken at time  $kT$  at the output of a filter matched to the overall impulse response  $h(t)$  when the input is the received signal  $r(t)$ , and  $x_k$  is a sample of the autocorrelation function of  $h(t)$ .

This clarifies that the computation of the likelihood function requires passing  $r(t)$  through a matched filter with impulse response  $h^*(-t)$  followed by processing of the sampled outputs of the matched filter. Next, the Viterbi algorithm is employed by evaluating the LLF recursively and discarding the unlikely sequences.

For practical reasons, the analog MF can be replaced with discrete transversal MF having a finite number of taps. To approximate the true MF characteristics, the number of taps of the discrete MF must include all the significant components of the overall impulse response. For a sampling rate of  $1/T_s = N/T$  at the output of the receiver filter,  $T_s$ -spaced taps may be sufficient to

assure the optimum performance of the MLSE receiver if the received signal one-sided bandwidth is limited to  $1/2T_s$ . Then, the equations (2.23) and (2.24) can be re-expressed as

$$y_k = y(kT) = \sum_{n=0}^{NK-1} r(nT_s) h^*(nT_s - kT), \quad (2.25)$$

$$x_k = x(kT) = \sum_{n=0}^{NK-1} h^*(nT_s) h(nT_s + kT), \quad (2.26)$$

where  $y_k$  and  $x_k$  are obtained by downsampling the outputs of the discrete transversal MF to the sampled values of the inputs  $r(t)$  and  $h(t)$ , respectively.

Now, an incremental metric is required to process the VA in a recursive fashion. Thus,  $\Lambda_{mn}$  is used to refer to the partial computation of the metric up to  $k = n$  for the  $m$ -th sequence (where  $n < K$ ), then

$$\Lambda_{mn} = 2 \operatorname{Re} \left[ \sum_{k=0}^n (a_k^m)^* y_k \right] - \sum_{k=0}^n \sum_{i=0}^n (a_k^m)^* x_{k-i} a_i^m. \quad (2.27)$$

For the VA,  $\Lambda_{mn}$  may be computed recursively from the previous partial sum for the same sequence,  $\Lambda_{m(n-1)}$ , as [15]

$$\Lambda_{mn} = \Lambda_{m(n-1)} + 2 \operatorname{Re} \left[ (a_n^m)^* y_n \right] - 2 \operatorname{Re} \left[ (a_n^m)^* \sum_{k=0}^{n-1} x_{n-k} a_k^m \right] - |a_n^m|^2 x_0. \quad (2.28)$$

The equation may be further simplified. Since  $a_k \in \{\pm 1\}$ , the last term will always yield the same value for a given channel characteristic and can be discarded. Further, the factor of 2 for the other two terms may be dropped. Since any practical channel response  $h(t)$  will span an interval of  $LT$  seconds,  $x_k$  will

be zero for  $|k| > L$ . Hence, the summation in the second term can be rewritten as

$\sum_{k=1}^L x_k a_{n-k}^m$ . Finally, the recursive metric calculation reduces to

$$\Lambda_{mn} = \Lambda_{m(n-1)} + \text{Re} \left\{ (a_n^m)^* \left[ y_n - \sum_{k=1}^L x_k a_{n-k}^m \right] \right\}. \quad (2.29)$$

The second term is nothing but the incremental metric that is employed in the VA for transitions in between the states. It should be noted that the complexity of the incremental metric depends critically on the summation in the second term, thus on the coefficients  $x_k$ . In other words, the incremental metric depends only on  $a_n^m, \dots, a_{n-L}^m$ , i.e., on the last  $L+1$  bits of the data sequence. Then, the summation term in the brackets can have  $2^L$  distinct values depending on the possible combination of the state vector  $S_n = (a_{n-1}, a_{n-2}, \dots, a_{n-L})$  which consists of the previous  $L$  binary bits.

Viterbi algorithm compares the metrics of all sequences going into the same state at each instant  $kT$  and choose a survivor with the largest metric. The process is repeated for each of the  $2^L$  states. For binary signalling, each survivor gives rise to two extended sequences, but these are then pruned back to single survivor path by metric comparison of the two incoming sequences to each state.

Finally, it must be noted that the critical parameter which determines the number of states and hence the complexity of the receiver is the number of significant component of  $h_k$ . In this study, it is assumed that the overall impulse response, including the effect of pulse shaping filter, channel and the receiver filter, spans a time interval of 3 symbols, i.e.,  $L$  is chosen to be 2. This simply corresponds to the  $2^2 = 4$  states in the Viterbi algorithm. This is discussed in Chapter 5.

## CHAPTER 3

### SYMBOL SYNCHRONIZATION REVIEW

#### 3.1. Introduction

Timing recovery is one of the most critical functions that are performed at the receiver of a synchronous digital communication system. The receiver must know not only the frequency at which the outputs of the demodulators are sampled, but also where to take the samples within each symbol interval.

In this chapter, firstly the definition of symbol synchronization is presented. Second, a review of symbol timing recovery (STR) methods is given to highlight the attributes. In the context of this review, a brief history of timing recovery with some applications on MSK signals is included. Finally, the maximum likelihood estimation of the timing recovery and the Modified Cramér-Rao Bound is presented.

##### 3.1.1. Symbol Timing Recovery

In a digital communication system, the output of the demodulator must be sampled periodically at the precise sampling time instants that minimize the detector error probability. The process of extracting the clock signal for determining the accurate locations of the maximum eye openings for reliable detection is usually called symbol synchronization or symbol timing recovery (STR). A circuit that is able to predict such locations is called a timing (or) clock synchronizer.

Figure 3.1 illustrates the block diagram of a typical baseband receiver model with a channel introducing an arbitrary delay  $\tau$ . The received signal is composed of signal plus noise:

$$r(t) = s(t - \tau) + w(t), \quad (3.1)$$

where  $w(t)$  is a white Gaussian noise process. The received waveform is first filtered to remove the out-of-band noise and then sampled at  $T$ -spaced instants,  $t_k = kT + \hat{\tau}$ , where  $\hat{\tau}$  is the timing epoch that accounts for the propagation time of the signal from the transmitter to the receiver.

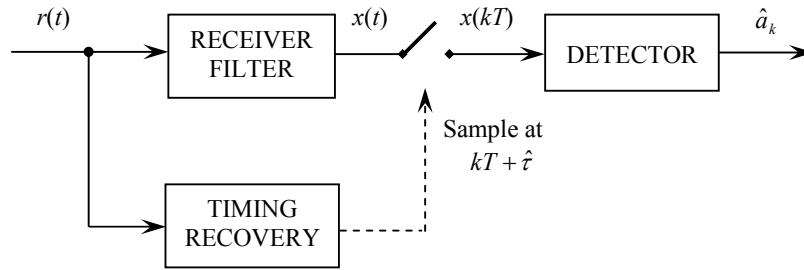


Figure 3.1 Typical block diagram of a baseband receiver.

The task of the timing recovery function, as stated, is to sample at the optimum sampling instants, which amounts to the maximum eye opening at the output of the receiver filter. This will ensure that the samples passed to the remaining receiver processes, including data detection, have the maximum available average signal-to-noise ratio (SNR) and hence a bit error rate (BER) as close as possible to optimum.

In selecting the STR scheme for a particular situation, some factors should be considered such as the modulation scheme being used, the transmission environment, the cost of implementation, the mode of the transmission (i.e. burst mode or continuous transmission) and physical limitations on size and power together with the complexity. The most important of these are the modulation scheme and the length of transmission. Next subsection gives some attention to

these facts within the consideration of the general forms of the timing recovery schemes.

### 3.1.2. Existing STR Schemes

The symbol synchronization literature is so vast as to comprise many technical papers with applications in diverse areas. This enormous knowledge has been elaborated in excellent books, the latest of which are by Meyr and Ascheid [21], Meyr, Moeneclaey and Fechtel [12], and Mengali and D'Andrea [22].

The process of symbol timing recovery (STR) varies according to the application. Existing symbol synchronizers appear in two main classes whether they are modeled with analog or digital methods. The former work on continuous-time waveforms where the latter perform the recovery of the timing epoch by operating on signal samples taken at a suitable rate. Since the proposed scheme basically resembles digital synchronizer schemes, in this general review of existing schemes the main emphasis is given to the digital timing recovery. Digital symbol synchronization methods are well established in the synchronization literature with many technical papers and the books by Meyr, Fechtel and Moeneclaey [12], and Mengali and D'Andrea [22].

As shown in Figures 3.2 and 3.3, the digital implementation of the synchronization process may take place using with either feedback (FB) or feedforward (FF) schemes [22]. The received signal can be sampled prior to or after the matched filter in both schemes. Each structure has its own particular merits. In both cases a low pass filter (LPF) limits the bandwidth of the received waveform. A typical feedback scheme is depicted in Figure 3.2. Here, the timing error detector (TED) takes the output of the timing corrector to generate an error signal  $e(k)$  proportional to the difference between  $\tau$  and its current estimate. The error signal is then filtered to reduce the variance of the timing error and the output is used to recursively update the timing estimates.

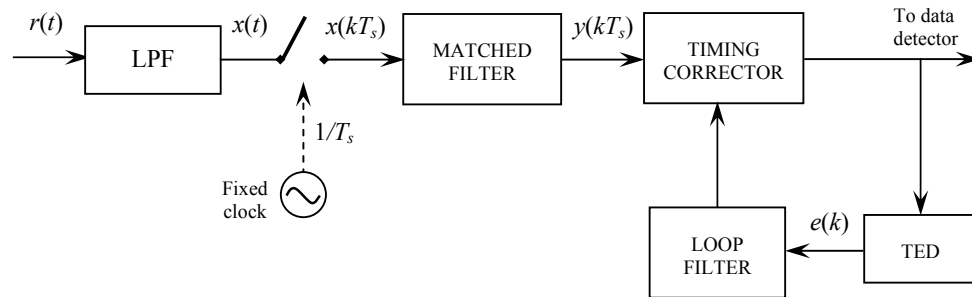


Figure 3.2 Feedback configuration.

On the other hand, feedforward methods derive an estimate of the timing epoch by applying a non-linear process within the STR circuit to the received signal samples. The estimate can then be used to adjust the sample timing to the optimum location. Generally, the tracking ability of the FB methods is superior to FF ones and they have less jitter when SNR is poor. But one can achieve fast acquisition times by employing FF schemes.

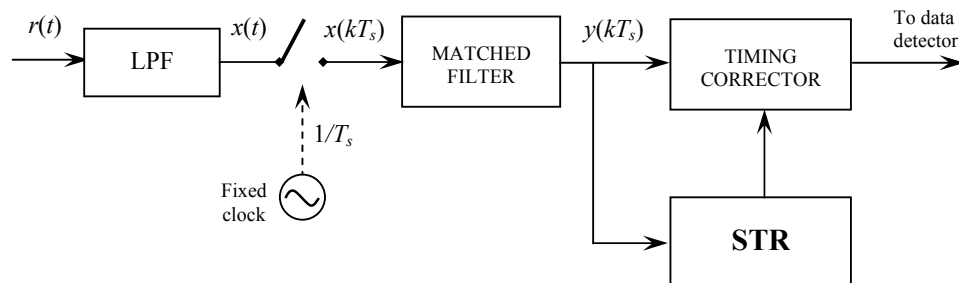


Figure 3.3 Feedforward configuration.

In the schemes described in Figures 3.2 and 3.3, a fixed clock whose ticks are not locked to the incoming data, controls the sampling. This is referred to as non-synchronized sampling. The sampling process can be performed also in a synchronized manner by feeding the number controlled oscillator (NCO) directly with the output of the STR circuit, as shown in Figure 3.4. Here the sampler is commanded by the NCO pulses at times  $\{t_k\}$ . Note that, as an example, the sampling process is performed after the MF and the analog MF in the figure may

be replaced by a digital MF inside the loop, as in the previous Figures 3.2 and 3.3. Moreover, synchronous sampling can be used both with feedback and feedforward schemes.

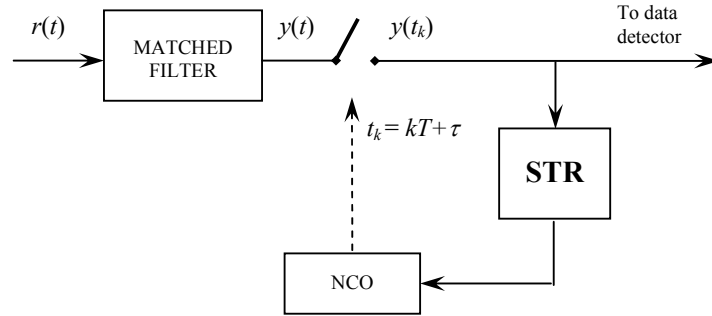


Figure 3.4 Synchronous sampling.

For completeness, it is valuable to mention about the timing correction block shown in Figures 3.2 and 3.3. Timing correction is generally performed with interpolators with the desired interpolation times  $\{t_k\}$ . It serves to provide the decision device with signal samples with the corrected timing values, i.e., with minimum intersymbol interference.

Also the timing synchronizers can be divided into two broad classes. First, synchronizers which use estimates of the received data values in obtaining the timing information are called decision-directed (DD) or data-aided (DA). In literature, DA timing recovery is generally referred to estimation of the timing epoch by using some preamble known to the receiver. The second class of synchronizers determines the timing phase error without using knowledge of the received data values. These are called non-decision-directed (NDD) or non-data-aided (NDA). Decision-directed STR schemes closely approach the performance bound but they are generally intolerant of carrier phase offset. Conversely, non-data-aided structures have poorer performance despite the fact that they are tolerant of carrier phase offset.

Since the second half of the last century, many timing recovery methods have been proposed with a steady performance improvement. Initially, timing synchronization information was transmitted on a separate channel. In the early 1960s, researchers have dwelled upon the investigation of new timing recovery schemes that all the transmitted energy is devoted to the transmission of the data signal, instead of dividing it between a data and a synchronization channel.

Early timing recovery methods were feedforward based and relied on the extraction of timing information from a discrete frequency component at the symbol rate. The frequency component is generally produced by feeding the baseband signal through a non-linearity, and then filtering the unwanted frequency components using a narrow bandpass filter or a phase locked loop (PLL). As the techniques for the analysis of the structures advanced through the 1970s, many classic papers were published mainly by Kobayashi in 1971 [23], Franks and Bubrouski in 1974 [24] and a very innovative one for synchronous digital receivers by Mueller and Muller in 1976 [9]. The tutorial paper by Franks in 1980 [25] described the symbol synchronization methods including the ones based on the maximum likelihood estimation criterion in the special issue of the IEEE Transactions on Communications (August 1980). This issue was devoted to synchronization and comprised many other papers with valuable contributions.

With the rapid advance in digital signal processing (DSP) devices, both the feedforward and feedback methods are increasingly being implemented in fully digital forms [12]. The papers mentioned above formed the bases of the extensive research on the digital synchronization. Further research has been devoted to the digital synchronization of nonlinear modulations formats, namely, continuous phase modulation (CPM) [1][26]. Next section gives the details of the research on symbol synchronization in MSK signals.

### **3.2. Symbol Synchronization in MSK Signals**

MSK is a subset of the continuous phase modulation (CPM) schemes (See Appendix A). Having constant envelope, they are very attractive in radio systems

employing low-cost non-linear power amplifiers. However, because of the implementation complexity and synchronization problems, not much attention is given to the symbol timing recovery of CPM signals especially for transmission in fading channels.

Symbol timing recovery for CPM signals has been first discussed by de Buda [3], specifically for minimum shift keying (MSK), where a nonlinearity is used to generate tones at the clock frequency. This algorithm was further analyzed in some papers and in [27] it has been shown that it can be used for any CPM signal. The problem with these Buda-like [26] synchronizers is their poor performance with the smoothed frequency pulses.

A decision-directed (DD) algorithm based on the maximum likelihood (ML) techniques is proposed in [28] and [7] using MSK modulation. Former provides the joint ML estimation of carrier phase, timing epoch and data, but suffers from spurious locks in the maximization of the likelihood function. The latter presents an all digital implementation with a feedforward carrier and clock synchronization. Although it is well suited for VLSI implementation, it includes some additional blocks to avoid hang-up problems.

In order to solve the problems related with the mentioned algorithms some NDA structures are developed. A feedback scheme is presented in [29] and its performance is compared with de Buda synchronizer. In [4]-[6], feedforward NDA algorithms are discussed. Two of these methods, proposed by Mehlan, Chen and Meyr [4] and Lambrette and Meyr [5], recover the clock signal in an ad hoc manner by passing the received signal samples through a nonlinearity and a digital filter. The algorithm behind this ad hoc scheme is obtained specifically for pure MSK and not applicable to any other CPM format. In a different approach, [6], the non-data-aided recovery is obtained by applying maximum likelihood methods. Although it is simple and seems suitable for burst mode transmission the algorithm is obtained under the assumption of low SNR. This results in the deviation from the desired performance even in the moderate SNR values.

Timing recovery in MSK signals with multipath fading channels has received scarce attention thus far. Although, it is widely believed that conventional clock synchronizers can be used even with fading channels, a closer look at the question may be worthwhile. In [4] and [8], the effects of a flat fading channel are taken in consideration with the symbol synchronizer employing nonlinearity and filtering in a feedforward manner. Also, the effect of frequency-selective channels is tested in [4], and a dramatic degradation is found in the bit error rate.

Apart from these attempts, some researchers intended to assess the error probability degradation due to synchronization imperfections. In [30], the effect of symbol timing errors on the BER is analyzed for linear modulations and given the comparison with MSK under the channel effects with a delay spread less than a symbol interval. It has been pointed out that MSK signal suffers from severe BER degradation in accordance with the increased delay spread. In [31], the effect of the timing errors is discussed when a coarse timing correction is employed in an MLSE receiver. It has been observed that the performance of the receiver is affected slightly from the timing errors when the delay spread of the channel does not exceed several symbol periods.

An example for the timing sensitivity of error probability of MSK signals is shown in Figure 3.5. The results are obtained under AWGN channel for different timing offset values. As is seen, for a value of  $\tau$  15% of the symbol period produces a signal energy loss less than 0.5 dB, but with a larger offset of  $0.3T$  a loss of 1 dB is noticeable. Thus, MSK signals may require well-designed symbol synchronizers in the presence of considerable timing errors. This is actually the case for the frequency-selective multipath fading channels.

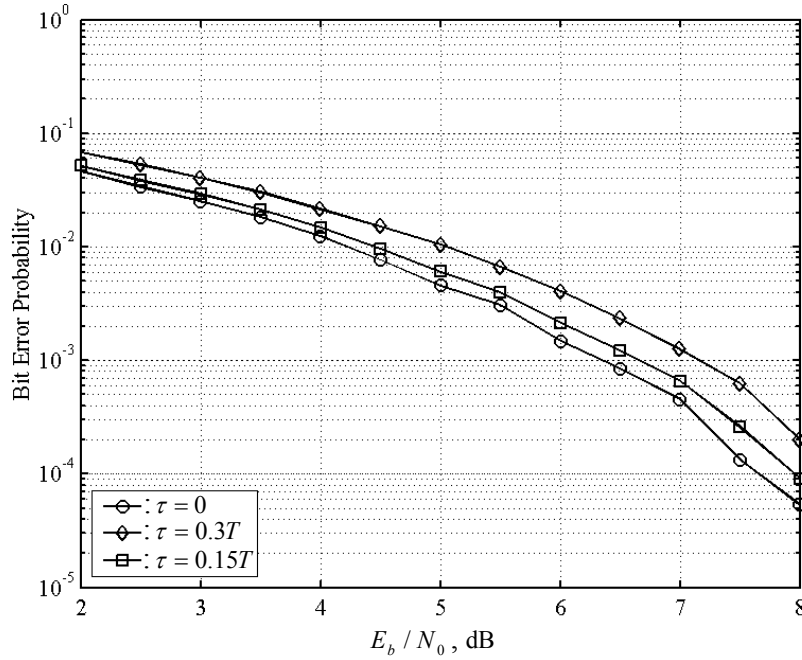


Figure 3.5 Effect of timing errors on MSK modulation.

### 3.3. Maximum Likelihood Timing Estimation

It is widely recognized that maximum likelihood (ML) estimation techniques offer a systematic and conceptually simple guide to the solution of synchronization problems and they provide optimum or nearly optimum solutions.

In this section the framework for maximum likelihood symbol timing recovery is established since most of the algorithms have been discovered by application of the ML estimation [25]. This is also the case for the proposed algorithm given in Section 4.3. The general formulation of the ML timing estimation is discussed in detail in [22] and [32].

Considering the baseband equivalent of the bandpass signal, the received signal in (3.1) can be described as

$$r(t) = s_l(t, \tau) + w(t), \quad (3.2)$$

where  $\tau$  represents an arbitrary delay introduced by the channel to the transmitted signal  $s_l(t)$ . The notation  $s_l(t, \tau)$  is adopted to stress the dependence of the signal on the timing epoch.  $w(t)$  is white Gaussian noise with spectral height  $N_0 / 2$ .

The ultimate goal of a symbol synchronizer is to estimate the most likely value of the timing epoch. This is accomplished when synchronizer maximizes the *a posteriori* probability for all values of  $\tau$  :

$$\hat{\tau}_{MAP} = \arg \max_{\tau} \{p_{\tau|r}(\tau | r(t))\} \quad (3.3)$$

given the observed signal  $r(t)$  [33].

ML estimation requires the determination of the signal  $r(t)$  which maximizes the conditional probability density function  $p_{r|s_l}(r(t) | s_l(t, \tau))$ , that is, the most likely signal,  $s_l(t, \tau)$ , which produces the received signal,  $r(t)$ , over a specific observation period  $T_0$ .

We can rewrite the *a posteriori* probability using Bayes' theorem:

$$p_{\tau|r}(\tau | r(t)) = p_{r|\tau}(r(t) | \tau) \frac{p_{\tau}(\tau)}{p_r(r(t))}, \quad (3.4)$$

where the probability density function (pdf)  $p_r(r(t))$  describes the probability that  $r(t)$  was received, and  $p_{\tau}(\tau)$  describes the probability that  $s_l(t, \tau)$  was transmitted with a delay of  $\tau$ . In this case  $p_{\tau}(\tau)$  is a constant assuming the time delay has a uniform pdf over the interval  $[0, T]$ . In addition,  $p_r(r(t))$  is simply a normalization constant.

Let  $\vec{r}$ ,  $\vec{s}_l(\tau)$  and  $\vec{w}$  be the vector representations of  $r(t)$ ,  $s_l(t, \tau)$  and  $w(t)$  over a complete orthonormal set  $\{\phi_i(t)\}_{i=1}^K$ . Then, the  $i$ -th component of  $\vec{r}$  is given by [33] as

$$r_i = \int_0^{T_0} r(t) \phi_i(t) dt . \quad (3.5)$$

Similarly,

$$s_{li}(\tau) = \int_0^{T_0} s_l(t, \tau) \phi_i(t) dt , \quad (3.6)$$

$$w_i = \int_0^{T_0} w(t) \phi_i(t) dt . \quad (3.7)$$

The standard form of the pdf for the sum of a known signal and AWGN, is

$$p_{r|\tau}(r_i | \tau) = \frac{1}{\sqrt{\pi N_0}} \exp \left[ \frac{-(r_i - s_{li}(\tau))^2}{N_0} \right]. \quad (3.8)$$

As the additive noise is considered to be white, the observations of noise,  $w_i$ 's, are independent, that is,

$$E\{w_i w_j\} = \frac{N_0}{2} \delta(i - j). \quad (3.9)$$

Hence, the pdf may be expanded over  $K$  components by taking the product of the pdfs for the individual sample observations and leads to the desired result

$$p_{r|\tau}(\vec{r} | \tau) = \frac{1}{(\sqrt{\pi N_0})^K} \prod_{i=1}^K \exp \left[ \frac{-(r_i - s_{li}(\tau))^2}{N_0} \right] \quad (3.10)$$

within the observation interval  $T_0$ . To simplify the likelihood function the natural logarithm may be taken, which after some rearrangement, results in

$$\ln[p_{r|\tau}(\vec{r} | \tau)] = -\frac{1}{N_0} \sum_{i=1}^K (r_i - s_{li}(\tau))^2 + C_K, \quad (3.11)$$

where

$$C_K = \ln \left[ \frac{1}{(\sqrt{\pi N_0})^K} \right]. \quad (3.12)$$

Equation (3.11) can be converted to the continuous time domain form by dropping the constant  $C_K$  as it is independent of the time delay and taking the limit as  $K \rightarrow \infty$ . Then, the result is

$$\Lambda_L(\vec{r} | \tau) = -\frac{1}{N_0} \int_{T_0} (r(t) - s_l(t, \tau))^2 dt, \quad (3.13)$$

where  $\Lambda_L(\vec{r} | \tau)$  is the continuous time log likelihood function (LLF). The squared term within the integral is a measure of the distance between the received and reference signals. Only the cross-correlation term in (3.13) contains useful information regarding the timing epoch.  $r^2(t)$  is independent of  $\tau$ , and the  $s_l^2(t, \tau)$  term is simply the power of the transmitted signal during the observation interval  $T_0$ . Consequently, the most likely timing offset  $\hat{\tau}$  can be expressed as the value of  $\tau$  which maximizes

$$\Lambda_L(\vec{r} | \tau) = \frac{2}{N_0} \int_{T_0} r(t)s_l(t, \tau)dt + const, \quad (3.14)$$

that is,

$$\hat{\tau} = \arg \max_{\tau} \{\Lambda_L(\vec{r} | \tau)\} = \arg \max_{\tau} \left\{ \frac{2}{N_0} \int_{T_0} r(t)s_l(t, \tau)dt \right\}. \quad (3.15)$$

The constant term is not included in (3.15), as it does not affect the maximization process. The final result will be used to explain the notion behind the proposed timing recovery algorithm in the next chapter.

### 3.4. Modified Cramér-Rao Bound

To compare the performance of synchronizers, establishing bounds to ultimate accuracy is an important goal. However, in their applications to synchronization problems some difficulties are encountered. The Modified Cramér-Rao Bound (MCRB) is introduced not to exhibit such difficulties [22].

Cramér-Rao Bound (CRB) is a fundamental lower bound on the variance of unbiased estimates. This bound is expressed as

$$\begin{aligned} \text{Var}\{\hat{\tau}(\vec{r}) - \tau\} &\geq \text{CRB}(\tau) \stackrel{\Delta}{=} \frac{1}{E_r \left\{ \left[ \frac{\partial^2 \ln \Lambda(\vec{r} | \tau)}{\partial \tau^2} \right] \right\}} \\ &= \frac{1}{E_r \left\{ \left[ \frac{\partial \ln \Lambda(\vec{r} | \tau)}{\partial \tau} \right]^2 \right\}}, \end{aligned} \quad (3.16)$$

where  $\vec{r}$  is the observation as defined in the previous section and  $E_r\{\cdot\}$  is the expectation with respect to  $\vec{r}$ . Any estimate that satisfies the bound is an efficient estimate [33]. Because of the difficulty of computing  $\Lambda(\vec{r} | \tau)$  for practical synchronization problems MCRB is used, which still applies to any unbiased estimator defined in the following form:

$$\text{Var}\{\hat{\tau}(\vec{r}) - \tau\} \geq \text{MCRB}(\tau) \quad (3.17)$$

with

$$\text{MCRB}(\tau) \stackrel{\Delta}{=} \frac{N_0/2}{E_u \left\{ \int_0^{T_0} \left| \frac{\partial s_l(t, \tau, \vec{u})}{\partial \tau} \right|^2 dt \right\}}, \quad (3.18)$$

in the case of baseband equivalent signals. In (3.18) the notation  $s_l(t, \tau, \vec{u})$  is used in place of  $s_l(t, \tau)$  and expectation  $E_u\{\cdot\}$  is defined over the unwanted parameters  $\vec{u}$  which may include the frequency offset, carrier phase and/or the data symbols.

The relation between the CRB and MCRB is addressed in [34] as

$$CRB(\tau) \geq MCRB(\tau). \quad (3.19)$$

The equality holds only in two special cases: where  $\vec{u}$  is perfectly known and the observation interval is much larger than the symbol interval or if there are no unwanted parameters. Equation (3.19) indicates that MCRB might be loose.

The MCRB for binary CPM signals is given in [22] as

$$\frac{1}{T^2} \times MCRB(\tau) = \frac{1}{8\pi^2 \zeta L_0} \frac{1}{E_s / N_0} \quad \text{where } \zeta \stackrel{\Delta}{=} h^2 T \int_{-\infty}^{\infty} g^2(t) dt. \quad (3.20)$$

$g(t)$  is the frequency pulse shape and  $L_0$  is the observation interval in terms of the symbol period.

For binary MSK signalling with the frequency pulse shape

$$g(t) = \begin{cases} \frac{1}{2T}, & 0 \leq t \leq T, \\ 0, & \text{elsewhere,} \end{cases} \quad (3.21)$$

(3.20) reduces to a simple form

$$\frac{1}{T^2} \times MCRB(\tau) = \frac{2}{\pi^2 L_0} \frac{1}{E_s / N_0}. \quad (3.22)$$

The relation given in (3.22) will be used for the comparison of the performance of the proposed STR scheme in the AWGN channel.

## CHAPTER 4

### A DD STR BASED ON MATCHED FILTERING FOR MSK SIGNALS

#### 4.1. Introduction

Transmission over frequency-selective fading channels necessitates specifically designed synchronizer structures and algorithms that are, in general, different from those for static channels. Feedforward approaches based on maximum likelihood (ML) estimation are good candidates and have received increasing attention [12][22][32]. They allow rapid acquisition and are well suited for burst-mode data transmission.

The proposed timing recovery scheme is based on the method of ML estimation of the timing epoch and does not employ any feedback loop. As a result, it does not suffer from hang-up problems which is common in feedback schemes. Correlation (matched filter) method is used for the recovery of the timing epoch. The cross-correlation between the received signal and the reference samples is interpolated and an iterative maximum search is performed for estimating the fractional delays.

The chapter starts with a study on “optimum timing phase” concept and some possible approaches. Next, the structure of the timing recovery scheme is presented with explaining the correlation (matched filter) method, interpolation and the iterative maximization process. Finally, a discussion on the performance of the proposed timing recovery scheme is given.

## 4.2. Optimum Value Criteria for Timing Phase

Although timing recovery is one of the most critical receiver functions in synchronous communication systems, not much attention is given for the investigation of the relation between the optimum timing phase criteria especially under the time-variant fading effects of the channel. The subject has received attention in early seventies and some possible optimum criteria have been presented in [9]-[11]. In [35], performance of some timing recovery algorithms are compared with the criterion proposed by Mazo [10] considering fading channel effects. In addition, a recent study [36] gives some attention to optimum timing values with emphasis on the timing sensitivity of MLSE receivers.

This section includes some possible criteria for establishing the notion behind optimum values for timing phase.

### 4.2.1. Mazo Criterion

In this criterion, optimum timing phase is defined as the one which results in the least MMSE, at the output of the equalizer. For most transmission systems the bandwidth is greater than  $1/2T$  where  $T$  is the symbol period. Therefore, when it is sampled at a rate  $1/T$ , the sampling phase will change the equivalent system response by cancelling or augmenting the aliased components. It has been shown by Mazo [10] that for a system consisting of a channel, a sampler and a forward linear equalizer the optimum timing phase is found by maximizing the equivalent channel magnitude response at the frequency  $1/2T$ , i.e., at the Nyquist band edge.

With the form of the received signal depicted in equation (2.18), the samples at the time instants  $t = kT + \tau$ , can be re-expressed in the absence of noise by

$$r_k(\tau) = \sum_n h_n(\tau) a_{k-n} . \quad (4.1)$$

To point out the dependence of the samples on  $\tau$ , the notation  $h_n(\tau) = h(nT + \tau)$  is used as in Section 3.3. These samples are related to their discrete Fourier transform as

$$h_n(\tau) = \int_{-\infty}^{\infty} H_{eq}(f, \tau) e^{j2\pi nT f} df, \quad (4.2)$$

where

$$H_{eq}(f, \tau) = \sum_n H(f + n/T) e^{-j2\pi(f+n/T)\tau}. \quad (4.3)$$

The exponential term in (4.3) reflects the effect of the timing phase. If the excess bandwidth of the sampled received signal is assumed to be less than 100%, then

$$H_{eq}(1/2T, \tau) = H(1/2T) e^{-j\pi\tau/T} + H(-1/2T) e^{j\pi\tau/T}. \quad (4.4)$$

According to the criterion proposed by Mazo [10], optimum timing phase is defined as  $\tau_{opt}$  that maximizes the cost function  $|H_{eq}(1/2T, \tau)|^2$  and approximately given by

$$\tau_{opt} = \frac{T}{2\pi} [\arg(H(1/2T)) - \arg(H(-1/2T))] + kT, \quad (4.5)$$

where  $k$  is any integer.

The equation derived by Mazo is nothing but the slope of the phase response between the frequencies  $\{-1/2T, 1/2T\}$ . Correspondingly, the timing phase behaviour given with this relation can be characterized by the slope of the phase response in a way given in the following formula:

$$\tau = \frac{T}{2\pi(f_1 - f_2)} [\arg(H(f_1)) - \arg(H(f_2))] + kT \quad (4.6)$$

with  $f_1 = -f_2 = 1/2T$ . This result directly gives the delay for linear phase systems, and in some sense may show the general tendency of the time-variant channel. Figures 4.1 and 4.2 show some examples for the timing values obtained by the equation (4.6) for different  $f_1$  and  $f_2$ .

In Figure 4.1, the variations of the timing phase are obtained for a multipath channel which is discussed in Chapter 5. Specifically, it corresponds to a variation with a mobile speed of 50 km/h and a carrier frequency of 900 MHz. The curves coincide in some specific interval and give the same delay. Other instants, the values of timing phase differ for different frequency pairs. Of course, this depends on the channel characteristics, but gives some information about the channel variations and the effects on optimum timing phase. Similar conclusions can be drawn for Figure 4.2. It gives the results of equation (4.6) under a faster channel variation.

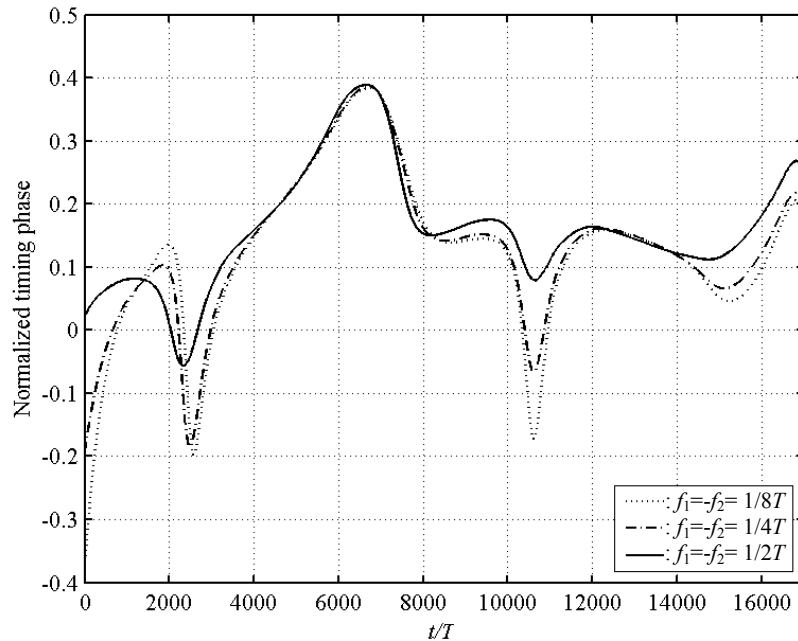


Figure 4.1 Normalized timing phase obtained from Mazo criterion ( $v = 50$  km/h,  $f_c = 900$  MHz).

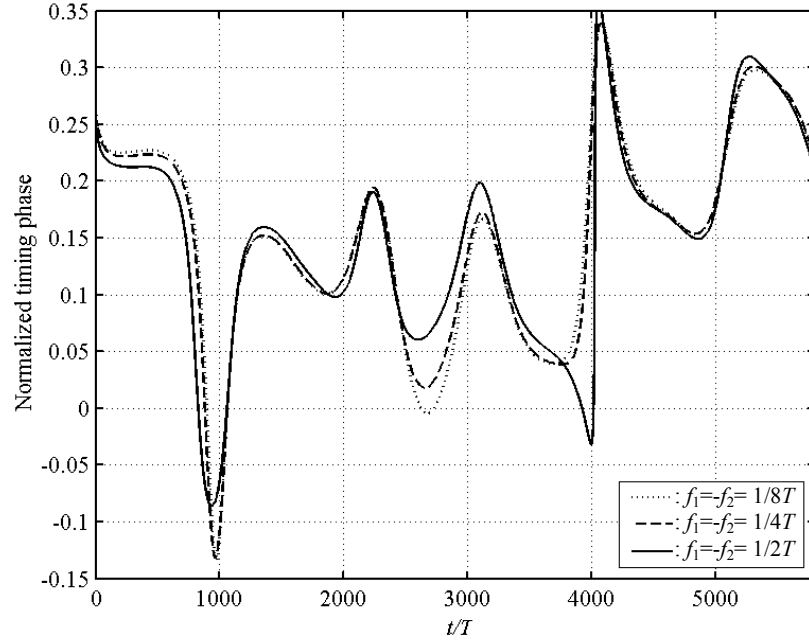


Figure 4.2 Normalized timing phase obtained from Mazo criterion ( $v = 90 \text{ km/h}$ ,  $f_c = 1800 \text{ MHz}$ ).

#### 4.2.2. Minimum Squared ISI (msISI) Criterion

Another criterion for the proper sampling is the determination of instants where we achieve minimum ISI, i.e., maximum eye opening. Considering again the general PAM form given in equation (2.18), the ideal set of samples are acquired when the overall impulse response can be expressed by  $h(0)=1$ ,  $h(kT)=0$ ,  $k \neq 0$ ; but this ideal set is never achieved in practice because of unknown channel distortion. Considering this, the distortion can be defined as

$$D(0) = \frac{\sum_{k \neq 0} |h(kT)|^2}{|h(0)|^2}. \quad (4.7)$$

By changing the sampling instant for  $h(t)$  other than taking  $t = 0$ , we obtain an appropriate measure for minimum distortion:

$$D(\tau) = \min_{\tau} \frac{\sum_{k \neq 0} |h(\tau + kT)|^2}{|h(\tau)|^2}. \quad (4.8)$$

This measure resembles minimization of the mean square distortion [9][11]. In [11], some possible distortion criteria for performance evaluation are discussed. Using (4.8) a possible optimum timing phase can be expressed as

$$\tau_{opt} = \arg \min_{\tau} \frac{\sum_{k \neq 0} |h(\tau + kT)|^2}{|h(\tau)|^2}. \quad (4.9)$$

The above criterion may allow us to choose a meaningful sampling epoch  $\tau$ , which results in minimum distortion. Because of the mathematical difficulty, an explicit expression is not presented as the one given for Mazo criterion in equation (4.5). Figures 4.3 and 4.4 show the results of the minimum squared ISI (msISI) criterion given in equation (4.9) and the comparison with the Mazo criterion with the same channels used in the previous figures.

It can be inferred that the two criteria track the channel variations and give close results for the timing epoch. With a detailed look the similarity between the msISI criterion and the timing estimates obtained by equation (4.6) with the frequencies  $f_1 = -f_2 = 1/4T$  is more clear especially in Figure 4.4. This is actually a channel dependent fact and one may encounter different similarities with different channel conditions.

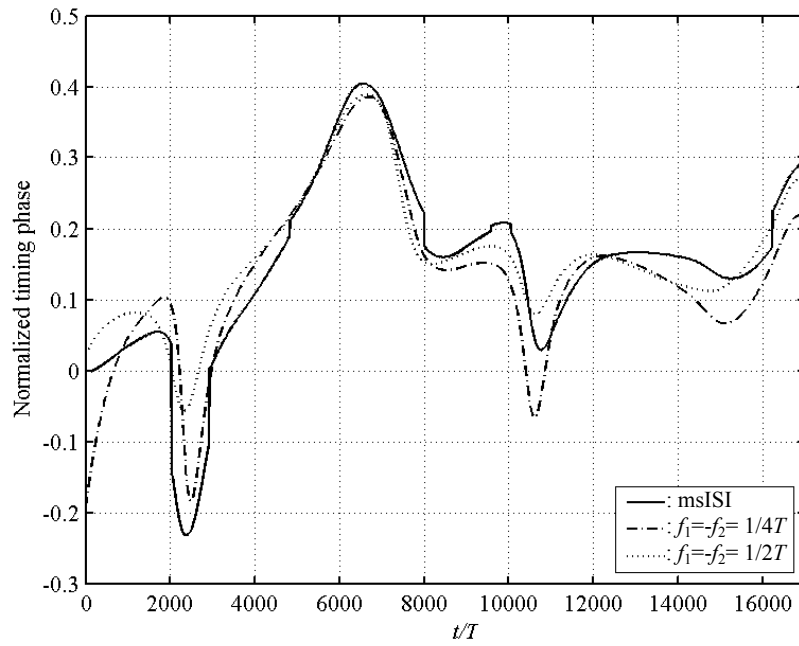


Figure 4.3 Comparison between the timing values obtained from msISI and Mazo criteria ( $v = 50 \text{ km/h}$ ,  $f_c = 900 \text{ MHz}$ ).

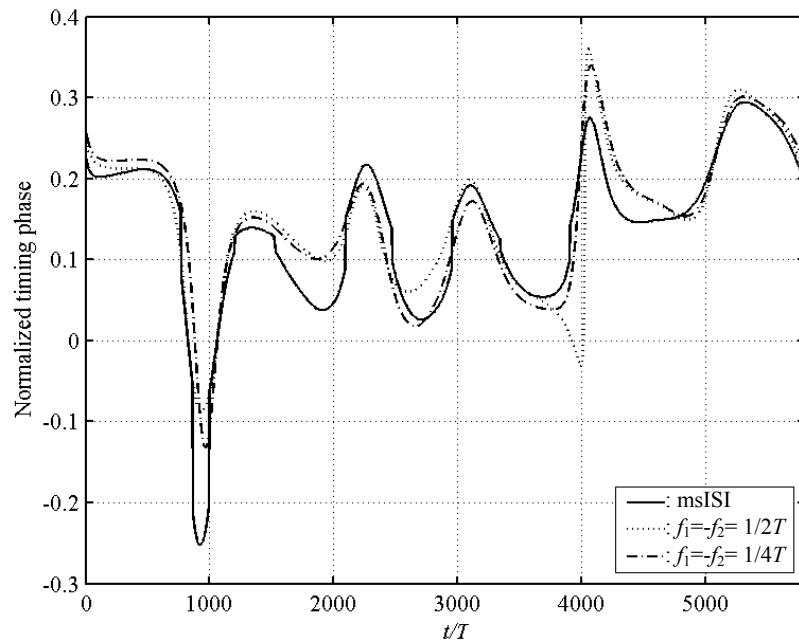


Figure 4.4 Comparison between the timing values obtained from msISI and Mazo criteria ( $v = 90 \text{ km/h}$ ,  $f_c = 1800 \text{ MHz}$ ).

It is interesting to note that the minimum squared ISI criterion defined by equation (4.9) physically tends to minimize the ISI energy in the received signal samples. This makes the msISI criterion much meaningful from the point of the proposed symbol synchronizer. The proposed method discussed in section 4.3 also has a tendency to increase the SNR value of the main component at the desired sampling instant. Hence, the tracking behaviour is to be similar.

### 4.2.3. Minimum BER Criterion

Without any doubt, the most meaningful criterion for optimum sampling is the minimization of the bit error probability. Considering the derivation given in Appendix B, it can be inferred that for MLSE receiver the timing values which maximize the minimum distance may be regarded as optimum. Hence, the following relation is the best criterion for the MLSE receiver:

$$\tau_{opt} = \arg \max_{\tau} \{d_{\min}^2(\tau)\}, \quad (4.10)$$

where

$$\begin{aligned} d_{\min}^2(\tau) &= E_{av}(\tau) \delta_{\min}^2 \\ &= E_{av}(\tau) \min_{\vec{\varepsilon} \in E} \left\{ \frac{1}{x_0} \sum_{i=k}^{k+l-1} \sum_{j=k}^{k+l-1} \varepsilon_i x_{i-j} \varepsilon_j \right\}. \end{aligned} \quad (4.11)$$

$d_{\min}^2(\tau)$  is the minimum distance as a function of the error vector  $\vec{\varepsilon}$  and the timing epoch  $\tau$  (See Appendix B).  $E_{av}(\tau)$  is the average energy which changes according to the sampling instant and  $\delta_{\min}^2$  is the minimum value of the normalized euclidean weight as defined in Appendix B.

Figure 4.5 shows the optimum timing values obtained from equation (4.10) using the same channel statistics as in Figure 4.3. The results completely differ from the ones obtained with the previous criteria. At a first glance, previously discussed criteria seems to be unsatisfactory. Hopefully, this inference does not much reflect the truth. The reason lies behind the timing sensitivity of the MLSE receiver as discussed in detail in [31] and [36]. In [36], the effects of timing errors

are studied on symbol-spaced MLSE receivers and the BER performance is investigated with different timing phase criteria. It has been shown that for bandlimited signals the timing appears to be uncritical with a coarse timing recovery scheme even if the received signal is sampled below the sampling rate. This is also discussed in [31] for GMSK signals and it is observed that with a free running clock and a coarse timing recovery technique, depending on the maximum energy search, the BER performance of an MLSE receiver varies slightly with a timing error at the sampling instants even in the presence of excess ISI. This directly explains the difference of the values obtained from the presented criteria.

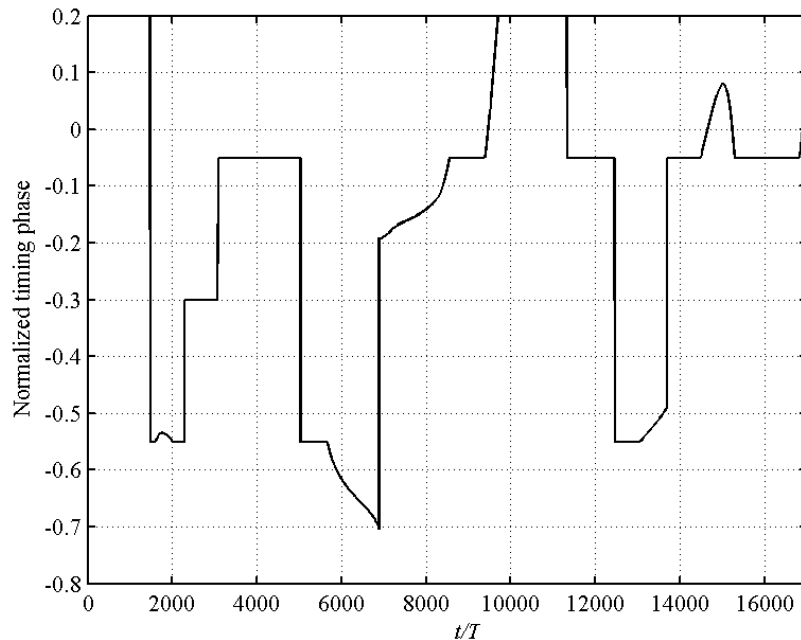


Figure 4.5 Timing values obtained from the maximization of the minimum distance.

Following this argument, the question arises about the degradation caused when the received signal is sampled with the recently mentioned minimum squared ISI (msISI) criterion. Figure 4.6 gives the minimum distance values for timing values obtained from equation (4.10) and the msISI criterion. The result is not surprising but specific for the channel used. It simply says that the distance is almost not affected. In other words, the energy of the received signal samples do

not change much in an interval including the timing instants determined by the two criteria. This specific result is given only for illustrating the behaviour of the mentioned criteria in terms of the BER performance. As stated in Chapter 5, the proposed scheme tracks the channel variations almost identically as the msISI criterion. Hence, it can be inferred that there will be no significant degradation from the point of BER performance of the receiver for the specified channels when the proposed scheme is employed for symbol synchronization.

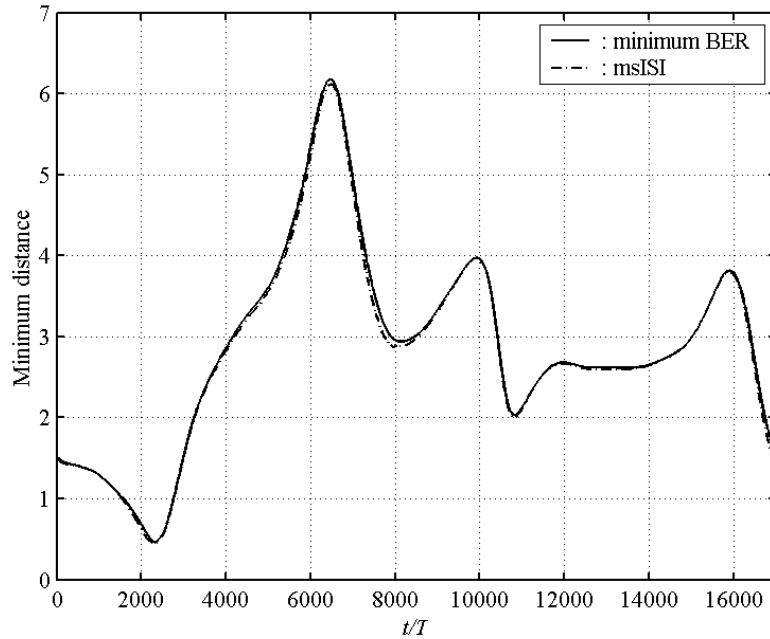


Figure 4.6 Minimum distance comparison between minimum BER and msISI criteria.

These comments can also be made by examining equations (4.10) and (4.11) in conjunction with the sampling theorem. In general, BER is dominated with single error events, which correspond to single bit errors in the error vector  $\bar{\varepsilon}$  in (B.6). That is, equation (4.11) becomes

$$d_{\min}^2(\tau) \approx E_{av}(\tau). \quad (4.12)$$

Then, the minimum distance gives the average energy in the sampled received signal. As seen in (4.12), the MLSE receiver behaves as an energy detector

algorithm, i.e., the optimum timing values correspond to the instants where the energy is maximized [31]. As a consequence, if the sampling rate with respect to the bandwidth of the overall impulse response  $h(t)$  does not violate the sampling theorem, the performance will be independent of the timing phase.

### 4.3. Proposed DD STR for MSK Signals

In this thesis study, a decision-directed timing recovery scheme is proposed which allows rapid acquisition and is robust in fading channel conditions. It simply employs correlation (matched filter) method based on maximum likelihood (ML) estimation of the timing epoch. For determining the fractional delays, classical interpolation and an iterative maximum search algorithm are used.

#### 4.3.1. Correlation (Matched Filter) Method

The method used for the recovery of the timing information is basically related to the estimation of arrival time of a pulse [33]. The notion behind this symbol timing estimation algorithm depends on the theory of maximum likelihood (ML) estimation. A large number of algorithms are presented previously which use several versions of ML estimators.

The proposed estimator does not give the estimates of the timing offset explicitly. It is based on the determination of the maximum value of the log likelihood function as a function of  $\tau$ , i.e.,

$$\hat{\tau} = \arg \max_{\tau} \{\Lambda_L(\tau)\}. \quad (4.13)$$

Let us rewrite the likelihood function (3.14) obtained in Section 3.3:

$$\Lambda_L(\tau) = \frac{2}{N_0} \int_{T_0} r(t) s_l(t - \tau) dt. \quad (4.14)$$

The integral in (4.14) is just a convolution operation and the likelihood function is simply the output of a filter with impulse response  $s_l(-t)$  and input  $r(t)$  over the observation interval  $T_0$ . Then, the estimate of the symbol timing

offset may be obtained by finding the timing instant which corresponds to the maximum of the output of the cross-correlation between the received and the reference signal samples. The correlation function can be expressed as

$$R(t) = \int_{T_0} r(u)s(u-t)du \quad (4.15)$$

and the proper sampling instant is given by

$$t_{smp} = \arg \max_t R(t) . \quad (4.16)$$

The correlation function can also be viewed as the output of a filter matched to reference signal when the input is the received signal. As a conclusion of the above relation, producing the replica of the received signal is enough for the estimation of the timing epoch even in the presence of the variations caused by multipath and noise. In the proposed synchronizer, the samples of the replica of the received signal are produced in a data-aided manner. In the acquisition mode of the synchronizer training sequence is employed. After the initial adjustment of the clock, the channel variations are tracked in a decision-directed manner using the decisions coming from the MLSE receiver.

In the tracking mode with the detection through the trellis in the Viterbi algorithm, the detector reliability depends on the decision delay. In other words, the delay between the current time and the time instant that the decisions are taken for timing recovery for symbol synchronization directly reflects the reliability of the detector. It is generally not clear where the break-even point is between having good decisions and short delays. This issue is the most important design criteria for the decision-directed algorithms. In VA, the decision delay for reliable detection is in the order of  $5L$  (where  $L$  is the memory of the overall impulse response) symbol intervals, which corresponds to 10 symbols in the proposed structure. However, such a delay in the timing recovery process degrades the tracking performance considerably in the presence of the channel variations. As a compromise, a smaller delay can be employed but this may also result in

performance degradation with fast channel variations. A reasonable solution to this is to take the best survivor sequence assuming that it is sufficiently reliable for timing recovery at the current time. These decisions are referred to as tentative decisions.

The tentative decisions are taken from the MLSE receiver and the matched filter is produced with the MSK modulated tentative decisions. Then, the timing epoch is estimated using the relation (4.16). This corresponds to the determination of the maximum of the matched filter output, i.e., the correlation function defined in (4.15). This is accomplished with interpolation and an iterative maximum search process as explained in the following sections.

### 4.3.2. Interpolation

As stated before, interpolation in receivers is generally employed to shift the received signal in time by the estimated timing offset value for fully digital applications [12]. In this study, the interpolation is used for approximating the correlation function other than determining the shifted sample values. Interpolation filters are usually based on FIR filter structures due to linear phase requirements. In the sequel, the classical interpolation method based on sampling theorem is used.

Classical interpolation is derived from the sampling theorem which states that a bandlimited signal with bandwidth  $B/2$  can be reconstructed exactly if  $f_s \geq B$ . If the bandlimited signal is sampled at the Nyquist rate, the recovery filter is the ideal rectangular filter. This rectangular filter which reconstructs the analog signal without aliasing is unique and unrealizable.

The ideal interpolation formula, which forms the basis of sampling theorem is, [37],

$$\tilde{R}(t) = \sum_{m=-\infty}^{\infty} R(mT_s) \frac{\sin\left(\frac{\pi}{T_s}(t - mT_s)\right)}{\frac{\pi}{T_s}(t - mT_s)}, \quad (4.17)$$

where  $T_s$  is the sampling period. The tilde indicates that the correlation function has been produced using interpolation.

A data window may be applied to (4.17) to reduce the distortion caused by the rectangular window and the associated Gibbs phenomena. Thus, if the signal is sampled at a rate higher than the Nyquist rate, various recovery filters may be designed.

In this thesis, raised cosine filter is used as the interpolation filter. The impulse response of the raised cosine filter may be written as

$$h_I(t) = \text{sinc}(2B_T t) \frac{\cos(2\pi\rho B_T t)}{1 - 16\rho^2 B_T^2 t^2}, \quad (4.18)$$

where  $B_T$  is the symmetry frequency and  $\rho$  is the roll-off factor. Figure 4.7 shows the impulse response of the raised cosine filter for different values of  $\rho$  with  $B_T = 1/2T$ .

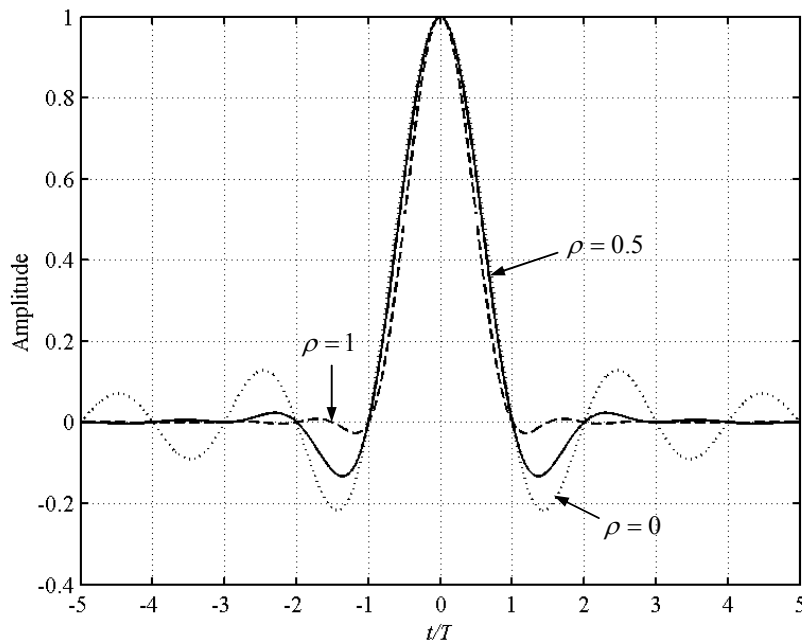


Figure 4.7 Impulse response of raised cosine filter.

According to the illustration of the samples in Figure 4.8, with an oversampling rate of  $N = T / T_s$ , the timing instants can be defined as

$$t_k = kT_s + \hat{\tau}, \quad (4.19)$$

where  $\hat{\tau}$  is the fractional delay and  $k$  is the index of the nearest sampling instant.

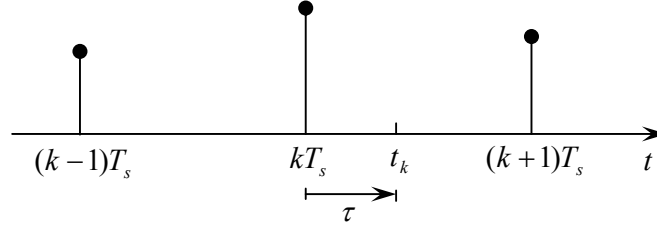


Figure 4.8 Illustration of  $k$  and  $\tau$  in determining the timing instant.

Using the notation in (4.19) the interpolation formula becomes

$$\tilde{R}(t_k) = \sum_{m=k-L_2}^{k+L_1} R(mT_s) h_l[(k-m)T_s + \tau] \quad (4.20)$$

with  $h_l(t)$  given in (4.18). Notice that, the summation in the equation (4.20) is truncated to a smaller length  $N_l = L_1 + L_2 + 1$  and this may distort the interpolated signal, unless  $N_l$  is sufficiently large. By changing the summation index in (4.20) we may obtain

$$\tilde{R}(t_k) = \sum_{i=-L_1}^{L_2} R[(k-i)T_s] h_l(iT_s + \tau). \quad (4.21)$$

The length of the interpolator,  $N_l = L_1 + L_2 + 1$ , used in simulations has been chosen to ensure that the variance of the timing estimates is tolerable. This issue is discussed in the last section.

### 4.3.3. Iterative Maximum Search

In determining the maximum of the correlation function, a simple and satisfactory iterative process based on Bisection Method [38] is employed. The iteration method presented here is similar to the one used in [32].

Bisection Method is a search algorithm with interval halving and a good candidate in iterative timing recovery process. Once the initial maximum has been located in an interval, the mid-point is taken as an estimate to  $\tau$ . Then, halving is performed, as will be explained, to refine the estimate, and the procedure is repeated until the interval is sufficiently small.

#### *Application of the Bisection Method to STR:*

The received baseband signal is sampled at a high enough sampling rate (to satisfy Nyquist sampling criterion) with samples stored in a buffer. Before the interpolation, the time interval  $[(k-1)T_s, (k+1)T_s]$  is determined where  $t = kT_s$  corresponds to the maximum of the correlation function.

After the determination of the interval  $[(k-1)T_s, (k+1)T_s]$ , including the maximum point, the two maximum values are selected from the samples at  $\{(k-1)T_s, kT_s, (k+1)T_s\}$  under the assumption that the optimum timing location lies between them. If the timing offset is not an integer multiple of the sampling period then the values of these samples differ in magnitude. Next, the procedure of halving is performed between the two selected sampling instants. The value of the correlation function is then evaluated for the new value of the timing offset and then the maximum two is selected among the three values of the samples.

The processes of “interpolation & calculation” of the correlation function and “maximum value selection” are then repeated until a sufficient number of iterations have been processed. At this stage, the timing value at which the correlation function has the maximum value is deemed to be the desired location. The iterative algorithm based on the Bisection Method is shown in Figure 4.9.

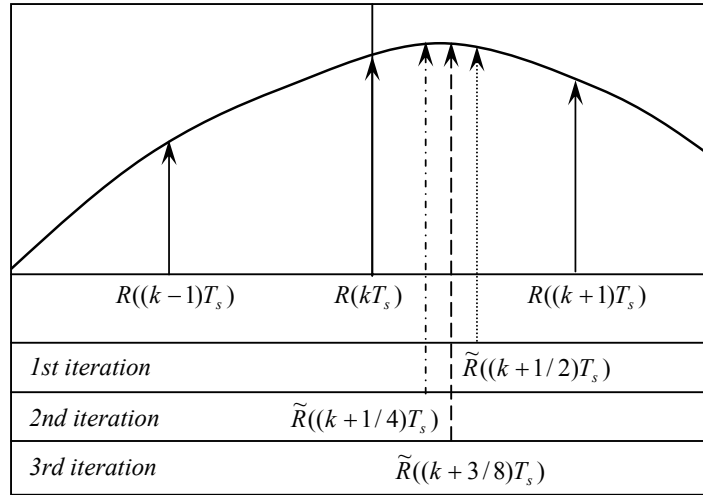


Figure 4.9 Illustration of the iteration process by Bisection Method.

#### 4.3.4. Discussion on Performance of the Proposed STR Scheme

The accuracy of the estimate obtained by the presented method is affected by a number of factors. In this subsection, these factors are discussed considering the acquisition mode of the synchronizer, i.e., the data values used for correlation are taken as known to the synchronizer. The results for the decision-directed mode of the synchronizer are presented in Chapter 5.

The correlation function is obtained by convolving the samples of the received signal with the corresponding reference signal, thus, oversampling rate will play an important role in the simulations. As given in [4], 99.5 % of the energy of the MSK signal is contained within a bandwidth of 1.5 times the symbol rate. Considering the bandwidth of the MSK signal and bearing in mind the fact that increasing the sampling rate will decrease the number of iterations in the maximum search process, sampling rate of  $T_s = T/N$  with  $N = 4$  may be a good choice. This results in an accuracy of  $1/128$  ( $1/N * 2^{n_{it}+1}$ ) of a symbol period only with  $n_{it} = 4$  iterations. In addition, the symmetry frequency of the interpolation filter is taken as  $2/T$  with the roll-off factor of 0.5 considering the bandwidth of the MSK signal.

Apart from the mentioned practical settings, the ultimate accuracy is limited by the variance of the timing estimate. From the point of the correlation method used for the timing recovery, the primary factor in obtaining estimates with low variance is the observation interval. The observation interval refers to the block length  $L_0$  used in the correlation which can be defined as the number of the symbols used in timing recovery, i.e.,  $T_0 = L_0 T$ . Figure 4.10 gives the relation of the variance to the block length for different SNR. As is seen, the block length of 30 symbols is a good choice even for low SNR values. Considering the moderate SNR values timing recovery can also be performed satisfactorily for smaller  $L_0$  values. In Chapter 5, the simulations are carried out generally for 30 symbols of block length. In addition, for some cases the comparison is given with  $L_0 = 20$ .

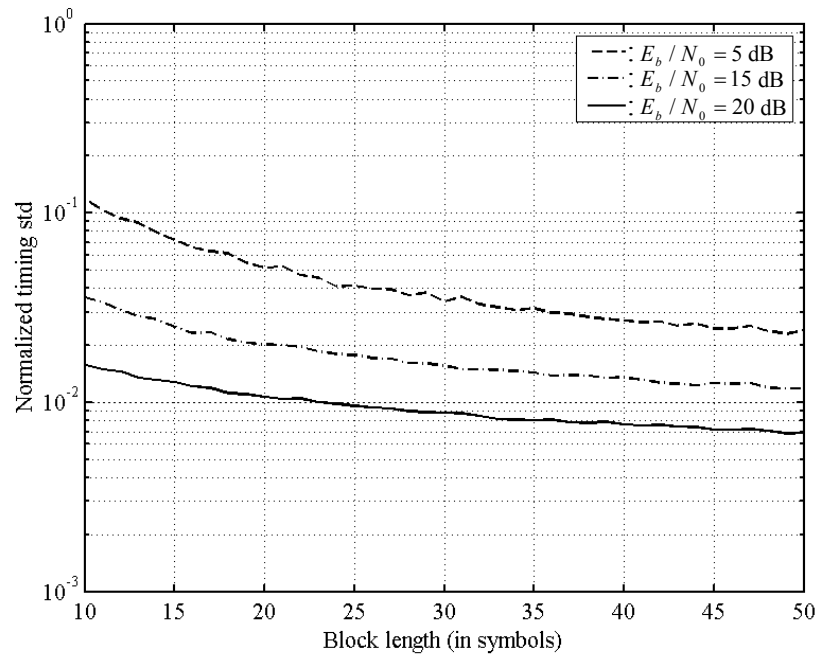


Figure 4.10 Normalized timing standard deviation for different SNR values.

Following determination of the block length for correlation, it is valuable to investigate the effect of the interpolation length. Figure 4.11 shows a typical matched filter output for a block length of 30. The useful information about the

timing epoch is in the main interval which contains the peak value at the matched filter output. Consequently, the components used in the interpolation should contain almost all the necessary samples; however, as the interval exceeds the useful part, timing errors may result. This can severely degrade the performance of the symbol synchronizer especially in low SNR and/or under fading channel effects.

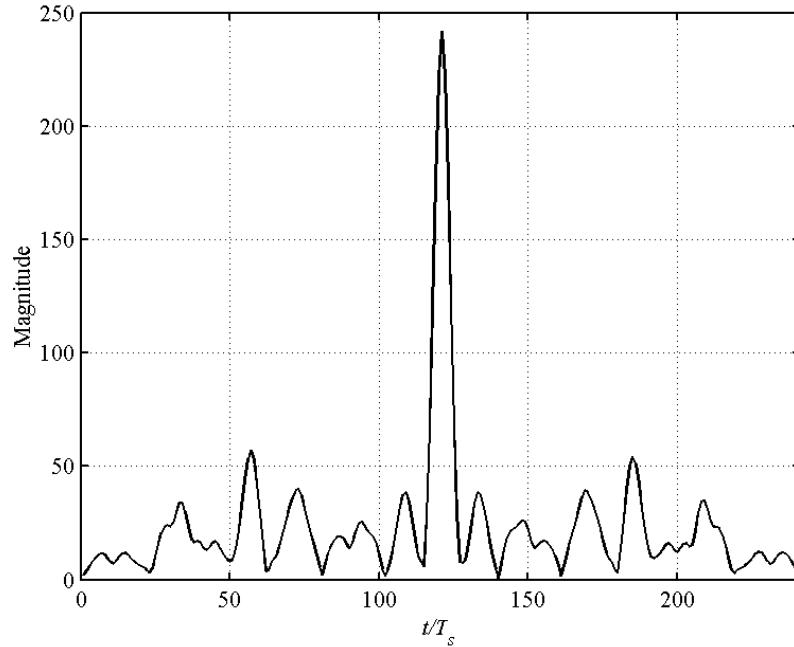


Figure 4.11 Matched filter output, SNR = 30 dB.

Tables 4.1 and 4.2 give the normalized standard deviation of the timing values for block lengths of 15 and 30 symbols, respectively. The variance is affected from the interpolation length much for the values of  $L_1 = L_2 = 1$ , i.e.,  $N_I = 3$ . Moreover, the values for 0 dB SNR in Table 4.1 implies that the timing estimates may not be satisfactory for a block length of 15 symbols whatever the interpolation length is. However, there is a remarkable decrease when the interpolation length is increased from 3 to 5 for the remaining cases. This trend does not continue as we increase the value of  $N_I$  and the results for the interpolation lengths of 5 and 7 do not much differ. Thus, it can be inferred that as

the value of  $N_I$  is increased further the variance does not change. This is actually the case for high SNR values.

Table 4.1 Normalized timing standard deviation for  $L_0 = 15$ .

	0 dB	10 dB	20 dB
$N_I = 3$	0.1729	0.1501	0.1486
$N_I = 5$	0.1555	0.0368	0.0112
$N_I = 7$	0.1531	0.0442	0.0127

The standard deviation of the timing estimate may attempt to increase as we increase  $N_I$  as in Table 4.1. This is because of the distortion in the useful interval which contains the peak of the correlation function for a shorter block length.

In Table 4.2 the variance does not change much for  $N_I = 5$  and  $N_I = 7$  as in Table 4.1, since the distortion is somehow compensated with increasing the block length. The slight difference results from the sensitivity inherent in the iteration process. With a larger number of iterations the performance may be improved further with an increase in the complexity. In Section 5.3, the effect of the block length together with the number of samples taken for interpolation is shown for decision-directed timing recovery in AWGN channel.

Table 4.2 Normalized timing standard deviation for  $L_0 = 30$ .

	0 dB	10 dB	20 dB
$N_I = 3$	0.1490	0.1488	0.1481
$N_I = 5$	0.0906	0.0256	$8.19 \cdot 10^{-3}$
$N_I = 7$	0.0917	0.0263	$9.186 \cdot 10^{-3}$

When the channel is fading and not constant over the block length, increasing the number of samples used in the interpolation may result in a larger augmentation in the variance compared to Table 4.2. Figure 4.12 shows a matched filter output in the presence of fading channel effects. The useful part around the peak of the matched filter output is narrower, but not a problem in case the block length is chosen long enough. This simply implies that even in time-variant channel conditions as we choose the observation interval long enough for the correlation, we obtain satisfactory results for small interpolation lengths.

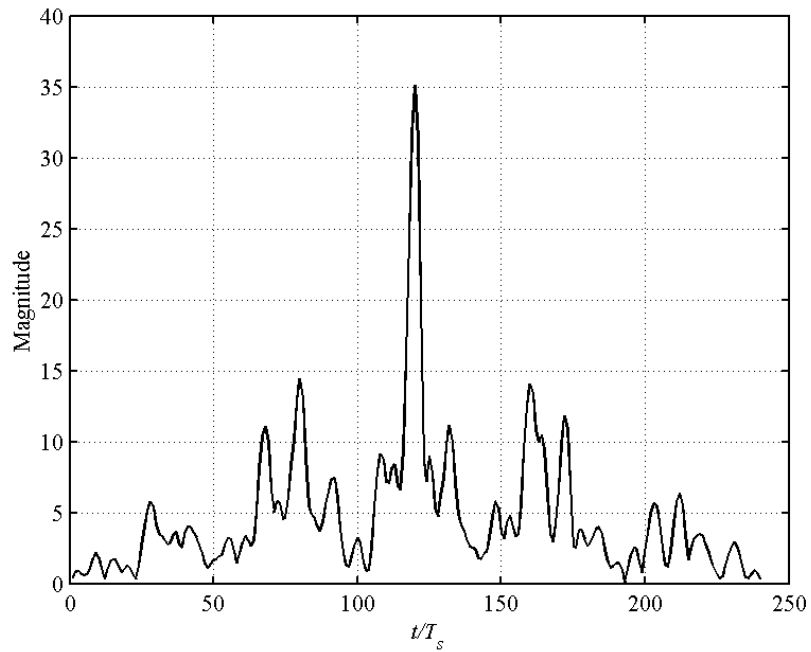


Figure 4.12 Matched filter output, SNR = 30 dB, fading channel.

Finally, Figure 4.13 summarizes the general flow in the timing recovery process. The received samples are first taken into the data buffer and then passed through the matched filter. Matched filter is obtained from the training sequence or the tentative decisions depending on the mode of the timing recovery process. Next, precise timing information is obtained by the iterative maximum search process using interpolator and Bisection Method. The tracking performance of this symbol synchronizer is discussed in the next chapter.

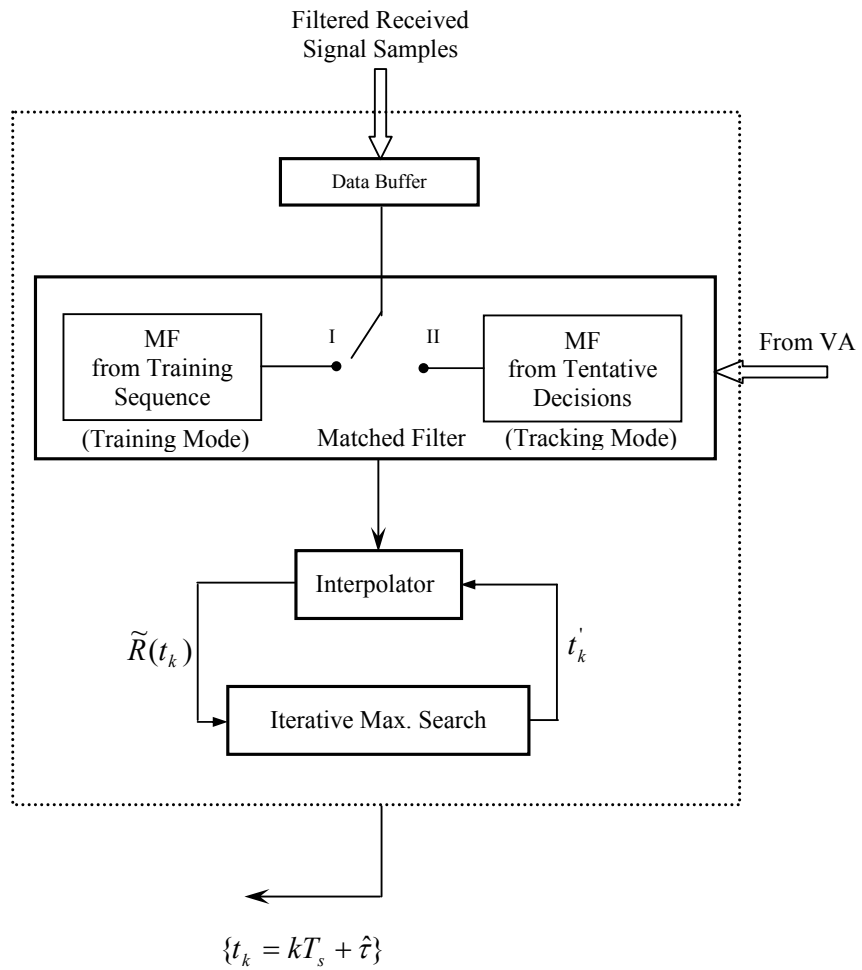


Figure 4.13 General flow in the proposed timing recovery scheme.

## CHAPTER 5

### SIMULATION & RESULTS

#### 5.1. Introduction

The proposed decision-directed symbol synchronizer has been simulated with software developed in MATLAB to observe the tracking performance under various channel conditions. Since MATLAB is based on discrete-time signals, the continuous-time signals are represented by their discrete samples taken at a rate greater than the Nyquist rate for a proper simulation.

In this chapter, the model of the simulated system is given. After introducing the general simulation chain, the channel model and the receiver structure are examined. Finally, the tracking ability of the synchronizer is given and compared with the minimum squared ISI (msISI) criterion mentioned in the previous chapter.

#### 5.2. Simulation Model of the Communication System

Firstly, the data burst is formed with randomly generated information sequence and a training sequence is placed in front of the burst for the acquisition of the initial timing information in the receiver. The data burst is modulated with the MSK modulator as shown in Figure 5.1. The output of the modulator is in the form of discrete samples with a time resolution of  $T/100$  which can be considered as almost continuous.

The modulated samples are then passed through the multipath fading channel. The simulated channel specifications are given in the next section. Following this, white Gaussian noise is added to the signal and passed to the

receiver. In the simulations bit-SNR is used as the performance criterion which is the ratio of the average received power to the spectral height of the noise.

The signal processing in the simulations is carried out in baseband and the RF part of the transmitter and the quadrature demodulation stage of the receiver are not simulated. The simulation chain of the system can be modeled as in Figure 5.1.

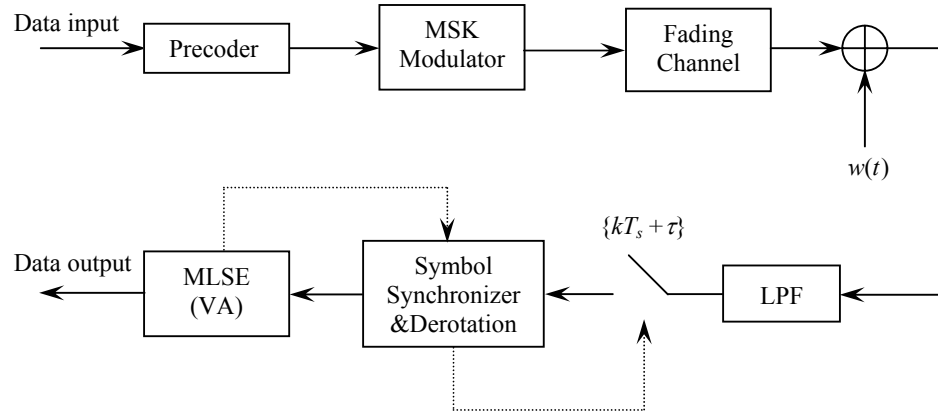


Figure 5.1 General block diagram of the simulated system.

### 5.2.1. Simulated Channel Specifications

In the simulation model, the complex baseband signal is transmitted through the tapped-delay-line (TDL) model of the time-variant frequency-selective fading channel [13], namely,

$$h_c(\Delta t; t) = \sum_{n=0}^{L_c-1} \alpha_n(t) \delta(\Delta t - n\Delta T). \quad (5.1)$$

$\Delta T$  is the time delay between the successive taps of the TDL model of the channel (also called the channel resolution) which generally satisfies  $\Delta T \leq 1/B$ , where  $B$  is the two-sided bandwidth of the MSK signal.  $L_c$  is the length of the channel in terms of  $\Delta T$ . For convenience, in the simulations,  $\Delta T$  is chosen simply as the sampling period  $T_s = T/4$ . The tap weight coefficients are adjusted

as explained in Chapter 2. The time spread of the channel is taken as  $L_c \Delta T = 2T$  with the symbol period of  $T = 3.5 \mu\text{s}$ . This corresponds to 9 discrete taps with exponentially decaying average power as in Figure 2.3.

In the simulations, two specific channel models are considered. One of them considers a TU radio channel encountered by a vehicle travelling at a speed of 50 km/h and communicating at a carrier frequency of 900 MHz. The second channel with the same power delay profile is a faster one with a speed of 90 km/h, where the carrier frequency is taken as 1800 MHz.

### 5.2.2. Receiver Structure

At the receiver part, the received signal is first passed through a low-pass filter (LPF) to reject the out-of-band components. The LPF used in the simulations is an 8-pole Butterworth filter with two-sided bandwidth  $B$ . The filtered signal is sampled with the rate  $T_s = T/4$  for proper timing extraction at the time instants determined by the symbol timing recovery circuit. This almost satisfies the Nyquist criterion for MSK signals (See Section 4.3.4).

The symbol synchronizer adjusts the initial timing by passing the signal samples through the filter matched to the MSK modulated training sequence, which is known by the receiver. In general, specific sequences with good cross-correlation properties are taken as the training sequences. In this study, training sequence is taken as a random sequence with the specified block length for the initial timing recovery. Next, the tracking of the timing phase with channel variations is performed in a decision-directed manner using the tentative decisions from the Viterbi algorithm. Tentative decisions are taken as the sequence corresponding to the best survivor path as explained in Section 4.3.1.

The rotational structure of the signal is removed after the synchronization using the precise timing instants, although the derotation function does not need to be synchronized due to the perfect estimate of the channel as stated in [18].

The derotated samples are fed to the MLSE receiver which includes a discrete transversal matched filter followed with the Viterbi processor. Since the channel is assumed to be perfectly known no restriction is made on the design of the MLSE receiver. In the Viterbi processor, the decoding operation is carried out at symbol rate so the output of the matched filter is downsampled to this.

The number of states in the Viterbi processor is determined by the number of significant components of the overall impulse response. The linearized pulse shape of the MSK signal spans a time interval of two symbols and the additional ISI introduced by the LPF to the overall system impulse response may be assumed negligible. Thus, with the channel impulse response described in the previous section, the number of significant components of the overall impulse response may be taken as 3, which corresponds to  $2^2 = 4$  states in the Viterbi algorithm.

### **5.3. Tracking Performance of the Symbol Synchronizer**

Before the discussion of the effects of channel variations on timing recovery, the performance of the synchronizer is tested in additive white Gaussian channel. Simulation of this channel involves the addition of the noise discarding the effects of the channel variations.

In Figure 5.2, the standard deviation of the timing estimate is compared with the MCRB given in Section 3.4. The bounds are plotted for two different block lengths. In Figures 5.3 and 5.4, the interpolation length is taken into account for the same block lengths and the comparison is given with MCRB.

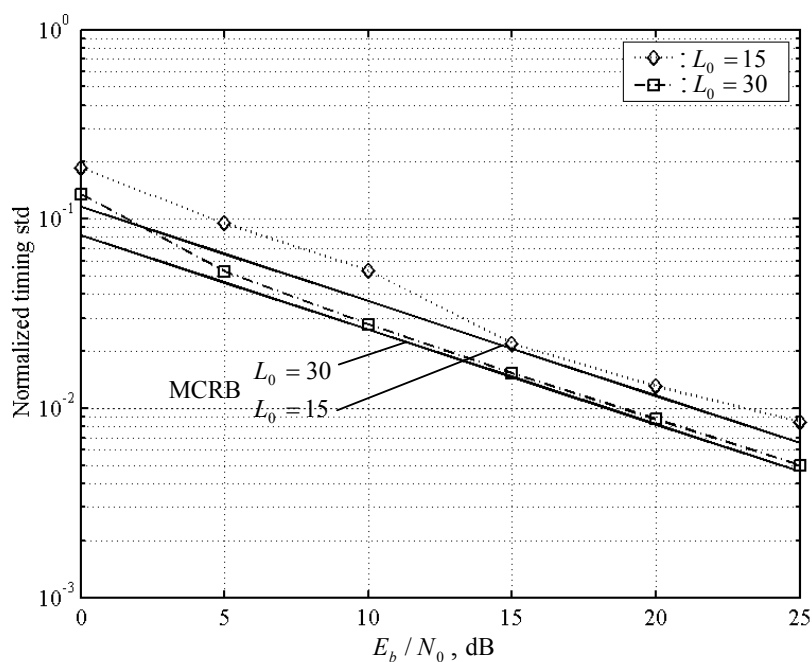


Figure 5.2 Performance of the symbol synchronizer in AWGN channel.

As seen from Figure 5.2, in both cases the estimates are close to the bounds and the synchronizer seems to give satisfactory estimates in AWGN channel. This is not a surprising but an important result to comment on severe effects of time-variant channels as will be discussed next. The deviation for both cases at low SNR values arises from the decision-directed nature of the proposed timing recovery scheme. As the number of errors increase in the tentative decisions, the variance deviates from the ultimate bound. However, the improvement with increasing the block length from 15 to 30 symbols is remarkable.

Figure 5.3 shows the deviation of the timing estimates for interpolation lengths,  $N_I = 5$  and  $N_I = 7$ . The results for moderate SNR values seem to be close to the MCRB bound but for low SNR cases the decision errors cause degradation in the performance. The effect of the interpolation length is negligible and this is also valid for the increased block length in Figure 5.4. Moreover, the effect of decision errors is compensated considerably.

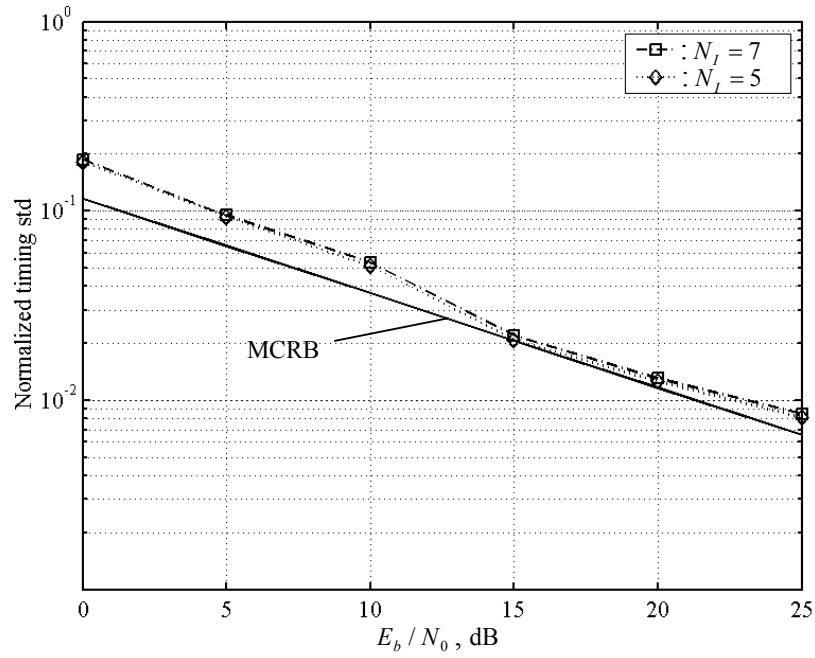


Figure 5.3 Performance of the symbol synchronizer for different interpolation lengths in AWGN channel ( $L_0 = 15$ ).

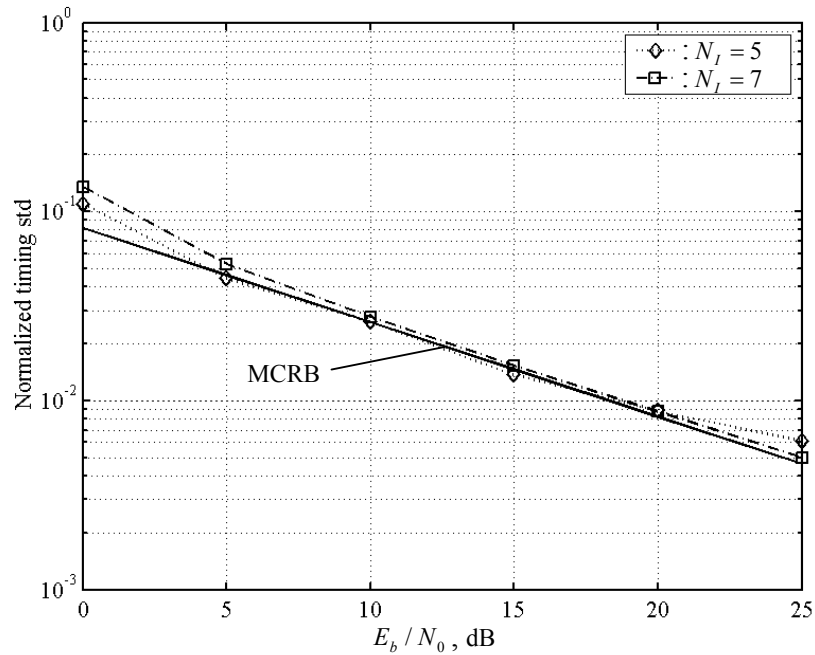


Figure 5.4 Performance of the symbol synchronizer for different interpolation lengths in AWGN channel ( $L_0 = 30$ ).

In the remaining part of the section the effects of the multipath fading channels are discussed. The tracking performance of the proposed timing recovery scheme is tested for the mentioned channel conditions at 30 dB SNR. As stated before, the initial recovery of the timing epoch is performed using a randomly generated training sequence with the specified block length. The block length is taken as 30 symbols and the interpolation is performed within an interval of  $N_I = 5$ , following the discussions made in Section 4.3.4 and in the previous paragraphs. In addition, for some cases the performance is given for the block length of  $L_0 = 20$  and SNR of 20 dB for comparison.

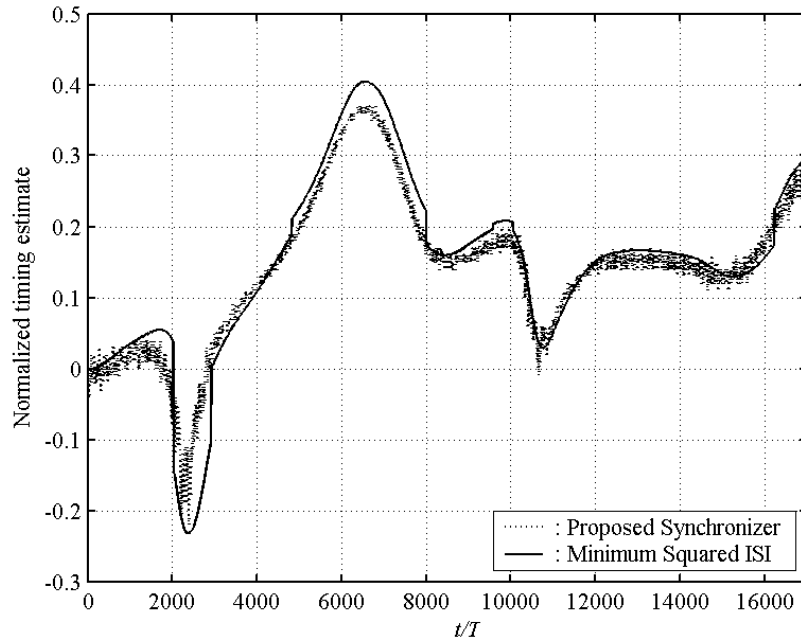


Figure 5.5 Tracking performance of the proposed scheme ( $L_0 = 30$ , SNR = 30 dB,  $v = 50$  km/h,  $f_c = 900$  MHz).

Figure 5.5 shows the tracking ability of the proposed symbol synchronizer for the channel also used for comparison of the possible optimum timing criteria in Chapter 4. The channel is TU model for 50 km/h mobile speed (TU50). It is clear that the proposed scheme tracks the channel very similar to the values obtained from the minimum squared ISI (msISI) criterion.

The same channel is simulated in Figures 5.6 and 5.7. In Figure 5.6, SNR is taken as 20 dB. Here, the tracking ability of the synchronizer is almost the same except a slight increase in the variance. In Figure 5.7, the block length is decreased to 20 symbols. However, the performance of the synchronizer is not affected much compared to the previous situations.

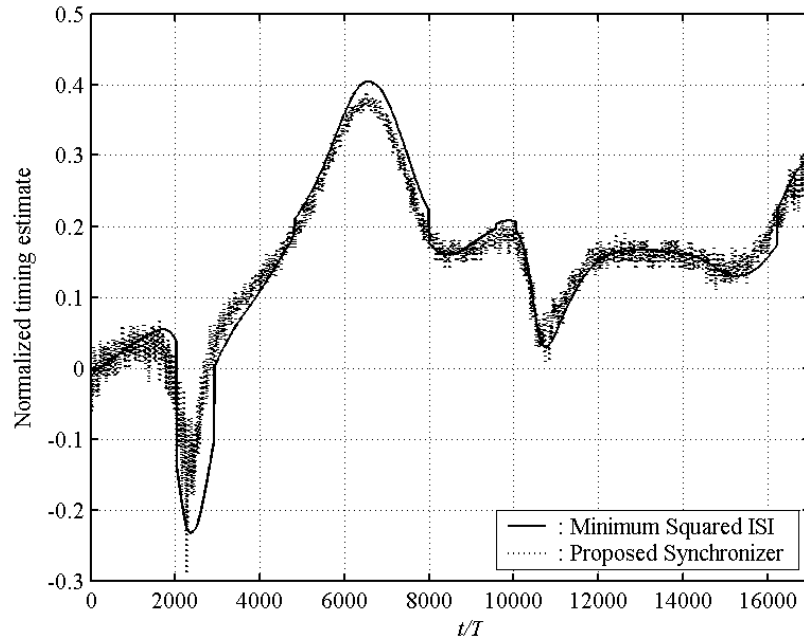


Figure 5.6 Tracking performance of the proposed scheme ( $L_0 = 30$ , SNR = 20 dB,  $v = 50$  km/h,  $f_c = 900$  MHz).

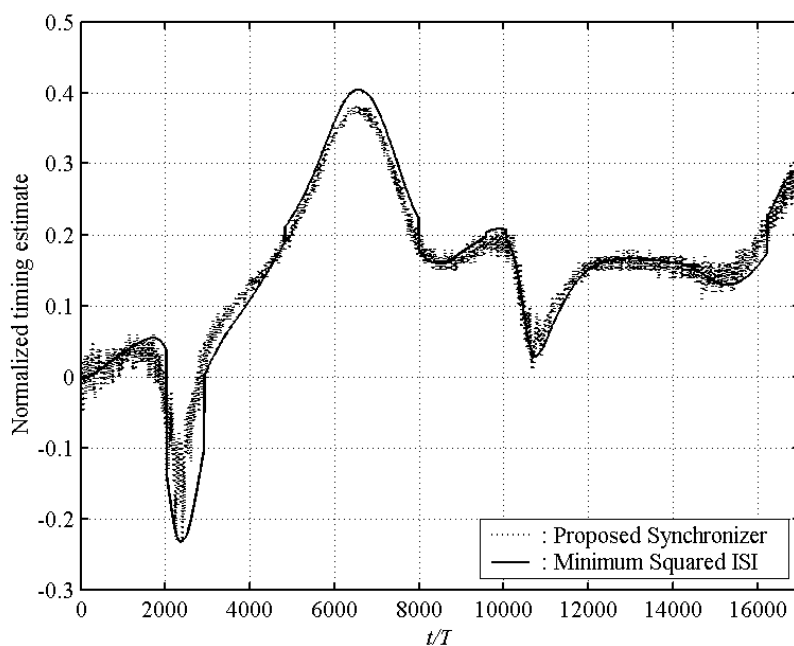


Figure 5.7 Tracking performance of the proposed scheme ( $L_0 = 20$ , SNR = 30 dB,  $v = 50$  km/h,  $f_c = 900$  MHz).

From the three figures mentioned, the performance of the proposed timing recovery scheme can be treated as successful. But the problems about timing recovery circuits arise in fading channels when deep fades occur in the main path. The following figures show the tracking ability of the proposed scheme for specific but informative cases considering the multipath fading channel specified with a vehicle speed of 90 km/h and a carrier frequency of 1800 MHz.

Figure 5.8 illustrates the effect of the fast variations. In this time period the channel variations are fast enough, but not much deep when a fade occurs in which the synchronizer may lose its tracking ability.

In Figure 5.9, the same interval for the channel is simulated for a block length of  $L_0 = 20$ . Although the channel varies faster, the effect of the block length is still negligible.

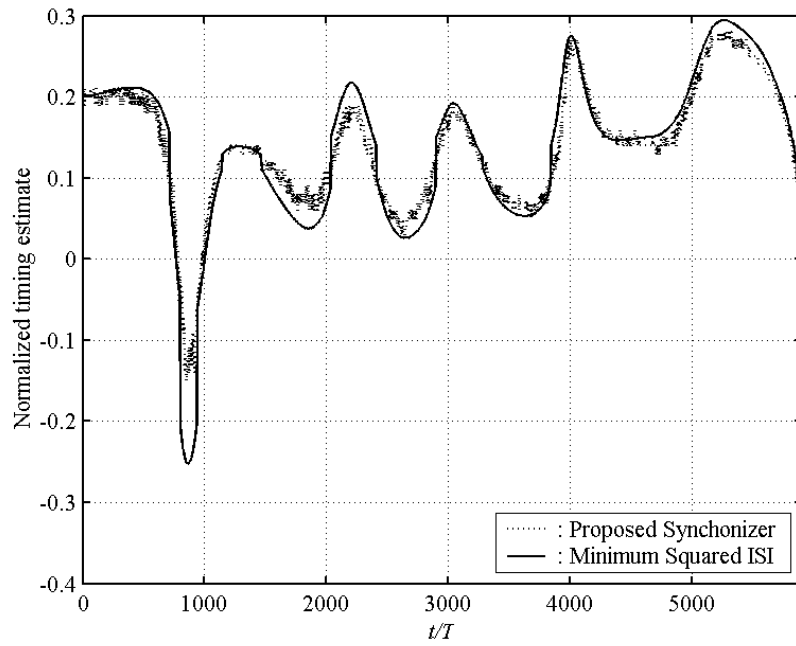


Figure 5.8 Tracking performance of the proposed scheme ( $L_0 = 30$ , SNR = 30 dB,  $v = 90$  km/h,  $f_c = 1800$  MHz).

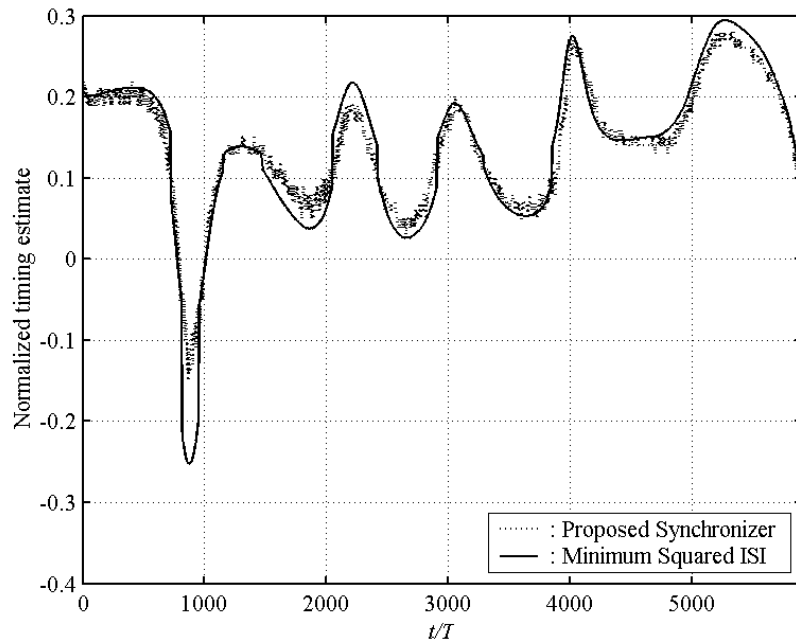


Figure 5.9 Tracking performance of the proposed scheme ( $L_0 = 20$ , SNR = 30 dB,  $v = 90$  km/h,  $f_c = 1800$  MHz).

In the following figures, more profound effects of the channel are shown. At some instants the channel comes across with deep fades. As seen from Figure 5.10, the proposed symbol synchronizer manages successfully with these effects, thanks to its ability to track the channel variations. The estimates are almost the same as the ones obtained from the msISI criterion, which is no longer surprising.

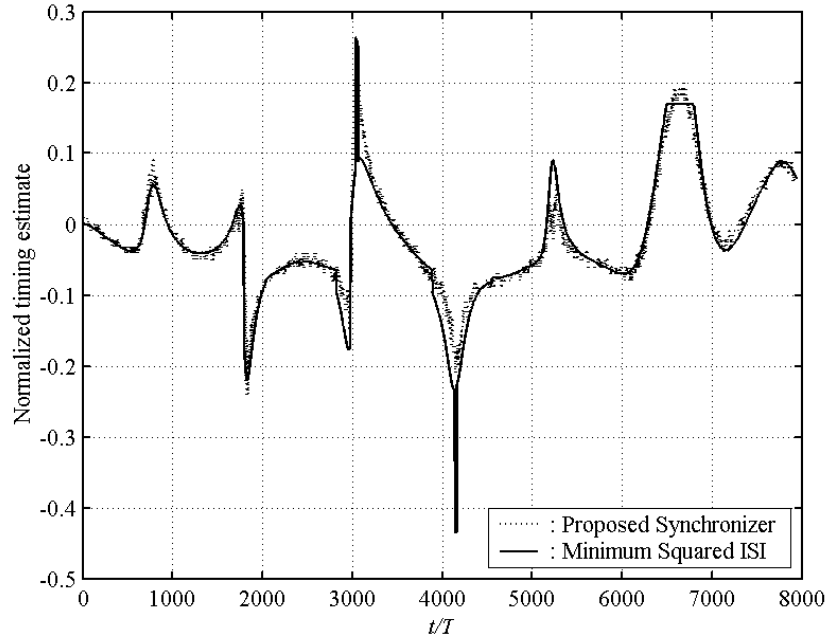


Figure 5.10 Tracking performance of the proposed scheme ( $L_0 = 30$ ,  $\text{SNR} = 30$  dB,  $v = 90$  km/h,  $f_c = 1800$  MHz).

In addition, the comparison is given between the msISI criterion and the Mazo criterion in Figure 5.11 to strengthen the claim that the timing recovery scheme tends to track the channel in the same way as the two possible optimum timing phase criteria. In this figure, the three curves do not completely coincide but detect the deep fades as the same as the proposed scheme.

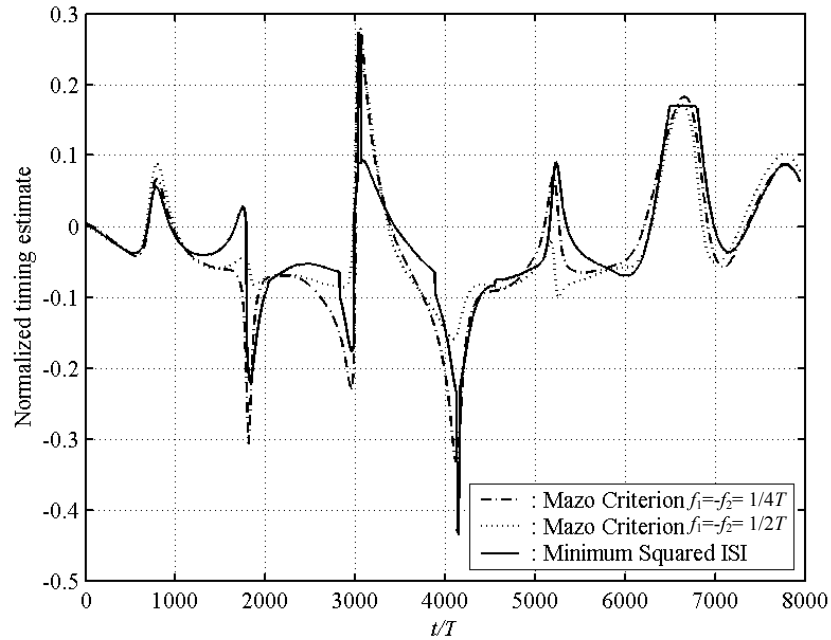


Figure 5.11 Comparison between msISI and Mazo criteria ( $L_0 = 30$ , SNR = 30 dB,  $v = 90$  km/h,  $f_c = 1800$  MHz).

In some situations the effects of deep fades become more crucial and result in highly catastrophic phenomena, namely, cycle slips. During a cycle slip, a burst of symbol errors is inevitable due to a symbol shift in the recovered sequence. Generally, cycle slips may occur both in feedforward and feedback synchronizers [12]. It has been observed in simulations that the proposed method has not yielded any cycle slip.

Figure 5.12 finalizes the discussion on the tracking performance of the proposed scheme. It illustrates the performance of the proposed scheme in the presence of a deep fade which may result in a cycle slip in conventional synchronizers. Notice that there occurs a change in the estimated timing epoch greater than a symbol period. It is interesting to note that the conventional synchronizers give the values of the timing phase within an interval  $[0, T]$ . Hence, such a jump in the timing estimate may not be tracked successfully, and may result in a cycle slip.

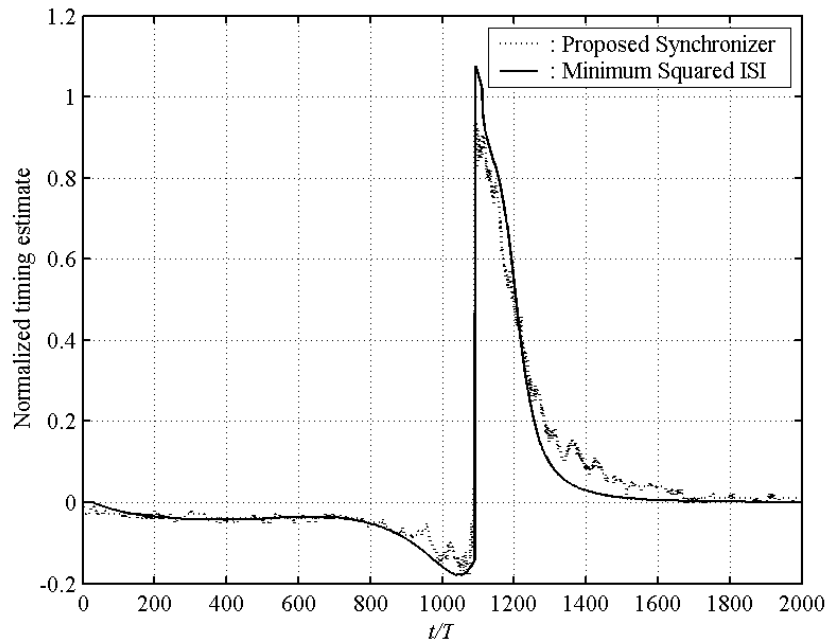


Figure 5.12 Tracking performance in the presence of a cycle slip ( $L_0 = 30$ , SNR = 30 dB,  $v = 90$  km/h,  $f_c = 1800$  MHz).

As a conclusion, the proposed decision-directed symbol synchronizer can be regarded as robust even in severe fading channel conditions. The timing epoch obtained from the proposed scheme tracks the channel variations close to the timing values obtained from the minimum squared ISI criterion and the proposed scheme eliminates the cycle slips successfully.

## CHAPTER 6

### CONCLUSION

Throughout this thesis study, it has been realized that although there have been an extensive amount of research on the area of symbol synchronization, there are still important issues left to investigate. With the demand for high-speed, high-quality and reliable communication, the need for proper symbol synchronization seems not to vanish.

In this thesis, a decision-directed STR scheme for MSK signals was proposed for the recovery of fractional delays with emphasis on multipath fading channel conditions. Correlation (matched filter) method based on maximum likelihood estimation was performed by using the samples of the received signal. Precise timing estimation was achieved by employing interpolation and an iterative maximum search process. The acquisition of the initial timing information was performed with a training sequence; while in the tracking mode tentative decisions from the MLSE receiver, implemented with VA, were used for the symbol timing recovery. In addition, in order to investigate the tracking performance of the proposed scheme, a study was carried out for optimum timing phase criteria and three possible criteria are examined, namely, the Mazo, the minimum squared ISI and the minimum BER criteria.

It has been observed that the proposed synchronizer tracks the timing epoch variations due to the time-variant multipath fading channel characteristics and gives almost the same results as the values obtained from the so-called minimum squared ISI criterion. However, this criterion was found to be suboptimum in the sense of minimization of the BER. In addition, BER

performance of the MLSE receiver was investigated from the timing accuracy point of view. As it is mentioned in the literature, the MLSE receiver generally requires maximum energy operation and for bandlimited signals, coarse timing might be sufficient even if the received signal is sampled below the Nyquist rate. Because of this reason, the fine timing recovery ability of the proposed scheme does not seem to be necessary from the point of the performance of an MLSE receiver. However, it tends to minimize the energy of the ISI present in the received signal and may allow a reduced state MLSE receiver. This statement does not guarantee the minimization of the bit error probability, however, the proposed timing recovery scheme at least guarantees the reduction of ISI.

Although the motivation of the study is and the results of the simulations are restricted to MSK signals, the proposed timing recovery scheme is modulation independent and applicable to any modulation type as CPM signals. It may be employed in both burst-mode and continuous transmission systems. The proposed scheme, because of its sensitive recovery of the fractional delays, can be used in repeaters and some network structures where fine timing estimation is important. In addition, with its ML based structure and decision-directed recovery process, the proposed scheme very successfully eliminates the possibility of cycle slips.

As a future work, the BER degradation may be investigated for the same receiver in the presence of excess ISI and different channel conditions. In addition, the performance of the synchronizer may be tested in unequalized systems which are preferred for low cost and low-complexity implementations. In unequalized systems ISI plays an important role, and with employing such a precise timing recovery scheme a considerable improvement is expected in BER performance.

## REFERENCES

- [1] A. N. D'Andrea, U. Mengali, and M. Morelli, "Symbol Timing Estimation with CPM Modulation," *IEEE Trans. Commun.*, vol. COM-44, pp. 1362-1372, Oct. 1996.
- [2] J. B. Anderson, T. Aulin, and C. E. Sundberg, *Digital Phase Modulation*, New York: Plenum Press, 1986.
- [3] R. de Buda, "Coherent Demodulation of Frequency Shift Keying with Low Deviation Ratio," *IEEE Trans. Commun.*, vol. COM-20, pp. 429-435, June 1972.
- [4] R. Melhan, Y. E. Chen, and H. Meyr, "A Fully Digital Feedforward MSK Demodulator with Joint Frequency Offset and Symbol Timing Estimation for Burst Mode Mobile Radio," *IEEE Trans. Veh. Technol.*, vol. VT-42, pp. 434-443, Nov. 1993.
- [5] U. Lambrette and H. Meyr, "Two Timing Recovery Algorithms for MSK," in *Proc. ICC'94*, New Orleans, LO, pp. 918-992, May 1994.
- [6] M. Morelli and G. M. Vitetta, "Joint Phase and Timing Recovery for MSK-Type Signals," *IEEE Trans. Commun.*, vol. COM-48, pp. 1997-1999, Dec. 2000.
- [7] G. Ascheid, M. Oerder, J. Stahl, and H. Meyr, "An All Digital Receiver Architecture for Bandwidth Efficient Transmission at High Data Rates," *IEEE Trans. Commun.*, vol. COM-37, pp. 804-813, Aug. 1989.
- [8] F. Patenaude, J. H. Lodge, and P. A. Galko, "Symbol Timing Tracking for Continuous Phase Modulation over Fast Flat-Fading Channels," *IEEE Trans. Veh. Technol.*, vol. VT-40, pp. 615-626, Aug. 1991.
- [9] K. H. Mueller and M. Muller, "Timing Recovery in Digital Synchronous Data Receivers," *IEEE Trans. Commun.*, vol. COM-24, pp. 516-531, May 1976.
- [10] J. E. Mazo, "Optimum Timing Phase for an Infinite Equalizer," *Bell Syst. Tech. J.*, vol. 54, pp. 189-201, 1975.

- [11] R. W. Lucky, J. Salz, and E. J. Weldon, Jr., *Principals of Data Communication*, New York: McGraw-Hill, 1968.
- [12] H. Meyr, M. Moeneclaey, and S. A. Fechtel, *Digital Communication Receivers – Synchronization, Channel Estimation and Signal Processing*, New York: John Wiley & Sons, 1998.
- [13] J. G. Proakis, *Digital Communications*, Singapore: McGraw-Hill, 1995.
- [14] P. A. Bello, “Characterization of Randomly Time-Variant Linear Channels,” *IEEE Trans. Commun. Sys.*, vol. CS-11, pp. 360-393, Dec. 1963.
- [15] Final Report of COST 207, “Digital Land Mobile Communication,” *publication of the Commission of the European Communities*, 1989.
- [16] P. A. Laurent, “Exact and Approximate Construction of Digital Phase Modulation by Superposition of Amplitude Modulated Pulses (AMP),” *IEEE Trans. Commun.*, vol. COM-34, pp. 150-160, Feb. 1986.
- [17] B. Canpolat, “Design and Simulation of an Adaptive MLSE Receiver for GSM System”, M.Sc. Thesis, Electrical and Electronics Eng. Dept., Middle East Technical University, Ankara, Feb. 1994.
- [18] A. Baier, “Derotation Techniques in Receivers for MSK-type CPM Signals”, in *Proc. 5<sup>th</sup> EUSIPCO*, Barcelona, Spain, pp. 1799-1802, Sept. 1990.
- [19] G. D. Forney, “Maximum Likelihood Sequence Estimation of Digital Sequences in the Presence of Intersymbol Interference,” *IEEE Trans. Inform. Theory*, vol. IT-18, pp. 363-378, May 1972.
- [20] G. Ungerboeck, “Adaptive Maximum Likelihood Sequence Estimation for Carrier Modulated Data Modulation Systems”, *IEEE Trans. Commun.*, vol. COM-22, pp. 624-636, May 1974.
- [21] H. Meyr and G. Ascheid, *Synchronization in Digital Communcatons*, vol. 1, New York: John Wiley & Sons, 1990.
- [22] U. Mengali and A. N. D’Andrea, *Synchronization Techniques for Digital Receivers*, New York: Plenum Press, 1997.
- [23] H. Kobayashi, “Simultaneous Adaptive Estimation and Decision Algorithm for Carrier Modulated Data Transmission Systems,” *IEEE Trans. Commun. Tech.*, vol. COM-19, pp. 268-280, June 1971.
- [24] L. E. Franks and J. P. Bubrouski, “Statistical Properties of Timing Jitter in a PAM Timing Recovery Scheme,” *IEEE Trans. Commun.*, vol. COM-22, pp. 913-920, July 1974.

- [25] L. E. Franks, "Carrier and Bit Synchronization in Data Communication – A Tutorial Review," *IEEE Trans. Commun.*, vol. COM-28, pp. 1107-1120, Aug. 1980.
- [26] A. N. D'Andrea, U. Mengali, and R. Reggiannini, "Carrier Phase and Clock Recovery for Continuous Phase Modulated Signals," *IEEE Trans. Commun.*, vol. COM-35, pp. 1095-1101, Oct. 1987.
- [27] T. Aulin and C. E. Sundberg, "Synchronization Properties of Continuous Phase Modulation," in *Proc. Int. Conf. Commun.*, Philadelphia, PA, pp. D7.1.1-D7.1.7, June 1982.
- [28] J. Huber and W. Liu, "Data-Aided Synchronization of Coherent CPM Receivers," *IEEE Trans. Commun.*, vol. COM-40, pp. 178-189, Jan. 1992.
- [29] A. N. D'Andrea, U. Mengali, and R. Reggiannini, "A Digital Approach to Clock Recovery in Generalized Minimum Shift Keying," *IEEE Trans. Veh. Technol.*, vol. VT-39, pp. 227-234, Aug. 1990.
- [30] S. Yoshida, S. Onoe, and F. Ikegami, "The Effect of Sample Timing on Bit Error Rate Performance in a Multipath Fading Channel," *IEEE Trans. Veh. Technol.*, vol. VT-35, pp. 168-174, Nov. 1986.
- [31] A. Baier, G. Heinrich, and U. Wellens, "Bit Synchronization and Timing Sensitivity in Adaptive Viterbi Equalizers for Narrowband-TDMA Digital Mobile Radio Systems," in *Proc. 38<sup>th</sup> IEEE Veh. Technol. Conf.*, Philadelphia, Pennsylvania, pp. 377-384, June 1988.
- [32] L. P. Sabel, "Maximum Likelihood Approach to Symbol Timing Recovery in Digital Communications," Ph.D. Thesis, Sch. of Elec. Eng., Univ. South Australia, South Australia, Oct. 1993.
- [33] H. L. Van Trees, *Detection, Estimation and Modulation Theory Part I*, New York: John Wiley & Sons, 1968.
- [34] A. N. D'Andrea, U. Mengali, and R. Reggiannini, "The Modified Cramér-Rao Bound and Its Applications to Synchronization Problems," *IEEE Trans. Commun.*, vol. COM-42, No: 2/3/4, pp. 1391-1399, Feb./March/April 1994.
- [35] Y. Tanik and S. Koç, "Performance Evaluation of Three Timing Recovery Algorithms in HF Channels," NATO-AGARD/EPP T-58 Support Project Final Report, May 1993.
- [36] P. Hoeher and S. Bahri, "Timing Sensitivity of Symbol-Spaced Trellis-Based Equalizers Applied to Frequency Selective Fading Channels," in *Proc. 7<sup>th</sup> Commun. Theory Mini-Conf.* in conjunction with *IEEE Globecom '98*, Sydney, Australia, pp. 88-93, Nov. 1998.

- [37] A. V. Oppenheim and R. W. Schaffer, *Discrete-Time Signal Processing*, Upper Saddle River, NJ: Prentice-Hall, 1999.
- [38] K. A. Sikorski, *Optimal Solution of Nonlinear Equations*, New York, NY: Oxford, 2001.

## APPENDIX A

### CPM SIGNALS

Continuous phase modulation (CPM) encompasses a class of signalling schemes that conserve and reduce signal energy and bandwidth at the same time. CPM is a constant envelope, nonlinear modulation method with memory. The constant envelope property of CPM schemes makes possible to use non-linear amplifiers. The phase is a continuous function of time since the data symbols modulate the instantaneous phase of the transmitted signal.

#### A.1. Signal Model

The complex envelope of a CPM signal is given by [2]

$$s_i(t) = \sqrt{\frac{2E_s}{T}} e^{j\phi(t, \vec{\alpha})}, \quad (\text{A.1})$$

where  $E_s$  is the signal energy per symbol,  $T$  is the symbol period,  $\vec{\alpha} = \{\alpha_i\}$  are data symbols from the alphabet  $\{\pm 1, \pm 3, \dots, \pm(M-1)\}$  and  $\phi(t, \vec{\alpha})$  is the information-bearing phase:

$$\phi(t, \vec{\alpha}) = 2\pi h \int \sum_{-\infty}^t \alpha_i g(t-iT) dt. \quad (\text{A.2})$$

The parameter  $h$  is the modulation index which takes on rational values as

$$h = \frac{2k}{p}, \quad (\text{A.3})$$

where  $k$  and  $p$  are intergers.  $g(t)$  is termed as the frequency pulse and the continuity of the phase implies that  $g(t)$  does not contain any impulses. The phase pulse  $q(t)$  is defined with the relation

$$q(t) = \int_{-\infty}^t g(\tau) d\tau, \quad -\infty < t < \infty, \quad (\text{A.4})$$

and is normalized in such a way that

$$q(t) = \begin{cases} 1/2, & t \geq LT, \\ 0, & t < 0. \end{cases} \quad (\text{A.5})$$

It is clear from (A.5) that the frequency pulse is nonzero in the interval  $t \in (0, LT)$ , where  $L$  is an integer called the correlation length. Modulation formats with  $L = 1$  are said to be *full-response* type whereas those with  $L > 1$  are *partial response* type.

By choosing different frequency pulses and varying the parameters  $h$  and  $M$ , a great variety of CPM schemes may be formed. In this thesis, the emphasis is given on a subset of CPM formats, namely, minimum shift keying (MSK). MSK corresponds to  $h = 1/2$ ,  $M = 2$  and a rectangular frequency pulse

$$g(t) = \begin{cases} 1/(2T), & 0 < t \leq T, \\ 0, & \textit{elsewhere}. \end{cases} \quad (\text{A.6})$$

Gaussian MSK (GMSK), which is used as the GSM and DECT modulation scheme, is obtained by letting  $h = 1/2$ ,  $M = 2$  and taking  $g(t)$  as the convolution of (A.6) with a Gaussian shaped pulse.

## A.2. Linearization of CPM Signals

This part gives an overview of the so-called *Laurent Expansion* [16]. This is a useful mathematical tool that provides good insight into the notion of MSK-type modulation and forms the basis for discussions made in this thesis study.

As stated recently, the frequency pulse is time-limited to the interval  $(0, LT)$  and satisfies the conditions

$$\int_0^{LT} g(\tau) d\tau = \frac{1}{2} \text{ and } g(t) = g(LT - t). \quad (\text{A.7})$$

As in [16], the complex baseband signal  $s_l(t)$  can be expressed as the sum of  $K = 2^{L-1}$  PAM signals, i.e.,

$$s_l(t) = \sqrt{\frac{2E_s}{T}} \sum_{k=0}^{K-1} \sum_{n=0}^{N-1} [e^{j\pi t a_{k,n}}] c_k(t - nT) \quad (\text{A.8})$$

over the interval  $t \in [0, NT]$ , where

$$\begin{aligned} a_{k,n} &= \sum_{i=0}^n \alpha_i - \sum_{j=1}^{L-1} \alpha_{n-j} \beta_{k,j} \\ &= a_{0,n} - \sum_{j=1}^{L-1} \alpha_{n-j} \beta_{k,j} \\ &= a_{0,n-L} + \sum_{j=1}^{L-1} \alpha_{n-j} (1 - \beta_{k,j}) + \alpha_n, \end{aligned} \quad (\text{A.9})$$

where the coefficient  $\beta_{k,j}$  is the  $j$ -th digit (0 or 1) in the binary representation of the interger  $k$ , i.e.,

$$k = \sum_{j=1}^{L-1} 2^{j-1} \beta_{k,j}, \quad k \in [0, K-1] \text{ and } \beta_{k,j} \in \{0,1\}. \quad (\text{A.10})$$

Finally,  $c_k(t)$ 's are given by

$$c_k(t) = s_o(t) \prod_{j=1}^{L-1} s_{j+L\beta_{k,j}}(t), \quad k \in [0, K-1], \quad (\text{A.11})$$

where

$$s_j(t) = \frac{\sin(\varphi(t+jT))}{\sin(\pi h)} = s_0(t+jT), \quad (\text{A.12})$$

$$\varphi(t) = \begin{cases} \phi(t), & 0 \leq t < LT, \\ \pi h - \phi(t-LT), & LT \leq t < 2LT, \\ 0, & \text{elsewhere,} \end{cases} \quad (\text{A.13})$$

and  $\phi(t) = 2\pi h \int_0^t g(\tau) d\tau$ .

For MSK,  $L=1$ ,  $h=1/2$ , and

$$g(t) = \begin{cases} \frac{1}{2T}, & 0 \leq t \leq T, \\ 0, & \text{elsewhere.} \end{cases} \quad (\text{A.14})$$

Therefore, we have  $K = 2^{L-1} = 1$ , so that the Laurent expansion of  $s_l(t)$  reduces to a single function, namely  $c_0(t)$ . This means that an MSK signal can be exactly represented as a PAM waveform. It can be seen from (A.11)-(A.14) that

$$c_0(t) = \begin{cases} \sin\left(\frac{\pi t}{2T}\right), & 0 \leq t < 2T, \\ 0, & \text{elsewhere.} \end{cases} \quad (\text{A.15})$$

This provides the well-known interpretation of MSK as offset-QPSK in which the pulse shape is a half-cycle sinusoid with 2 symbol period interval. The complex baseband representation for MSK is given by

$$s_l(t) = \sqrt{\frac{2E_s}{T}} \sum_{n=0}^{N-1} \left[ e^{j\frac{\pi}{2} a_{0,n}} \right] c_0(t-nT). \quad (\text{A.16})$$

## APPENDIX B

### ERROR PERFORMANCE OF THE MLSE RECEIVER

The error performance of the MLSE receiver is given in a form similar to the one in [13] adopted to the derivation presented by Ungerboeck [20]. Since the form given in Appendix A is the linear form of MSK, the approach for PAM signals can be used for the analysis.

With additive Gaussian noise and ISI, the metric given in (2.22) may be rewritten as

$$\Lambda_m \{\bar{a}\} = 2 \operatorname{Re} \left[ \sum_{k=0}^{K-1} a_k^m y_k \right] - \sum_{k=0}^{K-1} \sum_{i=0}^{K-1} a_k^m x_{k-i} a_i^m \quad (\text{B.1})$$

with

$$x_k = x(kT) = \int_{-\infty}^{\infty} h^*(t) h(t + kT) dt \quad (\text{B.2})$$

and

$$y_k = y(kT) = \int_{-\infty}^{\infty} r(t) h^*(t - kT) dt = \sum_l a_{k-l} x_l + \eta_k, \quad (\text{B.3})$$

where the symbols  $\{a_n\}$  may take the values  $\pm 1$ .  $\eta_k$ 's are the noise samples at the output of the matched filter. The trellis has  $2^L$  states at time  $k$ , as defined in Section 2.3.2, as

$$S_k(a_{k-1}, a_{k-2}, \dots, a_{k-L}). \quad (\text{B.4})$$

With this notation the estimated state at time  $k$  can be denoted by

$$\tilde{S}_k(\tilde{a}_{k-1}, \tilde{a}_{k-2}, \dots, \tilde{a}_{k-L}) \quad (\text{B.5})$$

with the corresponding estimated symbols  $\{\tilde{a}_n\}$  from the Viterbi algorithm. Through the trellis, suppose that the estimated path diverges from the correct path at time  $k$  and remerges with the correct path at time  $k+l$ , i.e.,  $\tilde{S}_k = S_k$  and  $\tilde{S}_{k+l} = S_{k+l}$ , but  $\tilde{S}_m \neq S_m$  for  $k < m < k+l$ . This is called an *error event* [5]. For the channel spanning an interval of  $L+1$  symbols, it follows that  $l \geq L+1$ .

In this error event, we have  $\tilde{a}_m = a_m$  for  $k-L \leq m \leq k-1$  and  $k+l-L \leq m \leq k+l-1$ . The corresponding error vector  $\vec{\varepsilon}$  is defined as

$$\vec{\varepsilon} = [\varepsilon_k \quad \varepsilon_{k+1} \quad \dots \quad \varepsilon_{k+l-L-1}] \quad (\text{B.6})$$

with

$$\varepsilon_j = \frac{1}{2}(a_j - \tilde{a}_j), \text{ and } \varepsilon_k \neq 0, \varepsilon_{k+l-L-1} \neq 0. \quad (\text{B.7})$$

The normalized elements  $\varepsilon_j$  take on the values  $\pm 1$  and there is no sequence of  $L$  consecutive elements that are zero.

To determine the probability of occurrence of the error event characterized by the error vector  $\vec{\varepsilon}$  given in (B.6), the procedure developed by Forney [19] is followed. Let  $E$  be the set of error events  $\vec{\varepsilon}$  permitted by the transmission code. For a distinct error event  $\vec{\varepsilon}$  to happen, the following three subevents  $E_1$ ,  $E_2$  and  $E_3$  must occur:

$$E_1 : \quad \text{at time } k, \tilde{S}_k = S_k;$$

$E_2$ : the sequence of information symbols  $(a_k, a_{k+1}, \dots, a_{k+l-L-1})$  is such that  $(\tilde{a}_k, \tilde{a}_{k+1}, \dots, \tilde{a}_{k+l-L-1}) = (a_k + \varepsilon_k, a_{k+1} + \varepsilon_{k+1}, \dots, a_{k+l-L-1} + \varepsilon_{k+l-L-1})$  is an allowable data sequence;

$E_3$ : for  $k \leq m < k+l$ , the sum of the branch metrics of the estimated path exceed the sum of the branch metrics of the correct path.

The probability of occurrence of  $E_3$  is

$$P(E_3) = P(\Lambda_m \{\tilde{a}\} < \Lambda_m \{\tilde{a} + \tilde{\varepsilon}\}). \quad (\text{B.8})$$

Substituting (B.3) into (B.1) and observing  $x_k = x_{-k}^*$ , (B.8) becomes

$$P(E_3) = P\left(\sum_{i=k}^{k+l-1} \sum_{j=k}^{k+l-1} \varepsilon_i x_{i-j} \varepsilon_j < 2 \operatorname{Re} \left\{ \sum_{i=k}^{k+l-1} \varepsilon_i \eta_i \right\}\right). \quad (\text{B.9})$$

The second term in the inequality is a normally distributed random variable with zero mean and variance [20]

$$\operatorname{var} \left\{ 2 \operatorname{Re} \left[ \sum_{i=k}^{k+l-1} \varepsilon_i \eta_i \right] \right\} = 4N_0 \delta^2(\tilde{\varepsilon}), \quad (\text{B.10})$$

where the normalized euclidean weight is defined as

$$\delta^2(\tilde{\varepsilon}) = \frac{1}{x_0} \sum_{i=k}^{k+l-1} \sum_{j=k}^{k+l-1} \varepsilon_i x_{i-j} \varepsilon_j. \quad (\text{B.11})$$

Hence, the probability of the subevent  $E_3$  becomes

$$P(E_3) = Q\left(\frac{1}{2} \sqrt{\gamma_{av} \delta^2(\tilde{\varepsilon})}\right), \quad (\text{B.12})$$

where  $\gamma_{av} = E_{av} / N_0$  denotes the average SNR. Considering the situation given in this study, the result needs some modification. In the case of different timing errors both the normalized euclidean weight and the average energy will differ. To proceed further for obtaining the general result for the probability of error, it is meaningful to define the distance as

$$d^2(\bar{\epsilon}; \tau) = E_{av}(\tau) \delta^2(\bar{\epsilon}; \tau). \quad (\text{B.13})$$

By substituting (B.13) in (B.12) we obtain

$$P(E_3) = Q\left(\frac{1}{2} \sqrt{\frac{d^2(\bar{\epsilon}; \tau)}{N_0}}\right). \quad (\text{B.14})$$

The probability of the subevent  $E_1$  is difficult to compute because of its dependence on the subevent  $E_3$  [13]. However,  $P(E_1 | E_3) = 1 - P(E)$ , where  $P(E)$  is the symbol error probability. Therefore, the probability  $P(E_1 | E_3)$  can be closely approximated by 1 in normal operating region. On the other hand, the probability of the subevent  $E_2$  depends only on the statistical properties of the input sequence. For binary signalling with equally probable and statistically independent symbols the probability of  $E_2$  becomes

$$P(E_2) = (1/2)^{l-L}. \quad (\text{B.15})$$

Observing (B.14), (B.15) and  $P(E_1 | E_3) \approx 1$ , the probability of the error event  $\bar{\epsilon}$  is upper bounded as

$$P(\bar{\epsilon}) \leq Q\left(\frac{1}{2} \sqrt{\frac{d^2(\bar{\epsilon}; \tau)}{N_0}}\right) \left(\frac{1}{2}\right)^{l-L}. \quad (\text{B.16})$$

Let  $E_\delta$  be the subevent of  $E$  containing all error events  $\bar{\varepsilon}$  with distance  $\delta(\bar{\varepsilon}) = \delta$ . By defining  $\Delta$  as the all possible values of  $\delta$ , the probability of error is upper bounded by

$$P(E) = \sum_{\bar{\varepsilon} \in E} P(\bar{\varepsilon}) \leq \sum_{\delta \in \Delta} Q\left(\frac{1}{2} \sqrt{\frac{d^2(\bar{\varepsilon}; \tau)}{N_0}}\right) \sum_{\bar{\varepsilon} \in E_\delta} \left(\frac{1}{2}\right)^{l-L}. \quad (\text{B.17})$$

Due to the steep decrease of  $Q(x)$ ,  $P(E)$  is dominated by the term corresponding to the minimum value of  $\delta$  denoted by  $\delta_{\min}$  for a given value of  $\tau$ . Hence, the bit error probability approaches asymptotically

$$P(E) \approx Q\left(\frac{1}{2} \sqrt{\frac{d_{\min}^2(\tau)}{N_0}}\right) \sum_{\bar{\varepsilon} \in E_{\delta_{\min}}} \left(\frac{1}{2}\right)^{l-L}, \quad (\text{B.18})$$

where

$$\begin{aligned} d_{\min}^2(\tau) &= E_{av}(\tau) \delta_{\min}^2 \\ &= E_{av}(\tau) \min_{\bar{\varepsilon} \in E} \left\{ \frac{1}{x_0} \sum_{i=k}^{k+l-1} \sum_{j=k}^{k+l-1} \varepsilon_i x_{i-j} \varepsilon_j \right\}. \end{aligned} \quad (\text{B.19})$$